ON DYNAMICS OF MULTI-MODE SYSTEMS:

PROCESS DAMPING EFFECT & FRF MODIFICATION

by

YASER MOHAMMADI

Submitted to the Graduate School of Engineering and Natural Sciences

in partial fulfillment of the requirements for the degree of

Master of Science

Sabancı University

July 2017

ON DYNAMICS OF MULTI-MODE SYSTEMS:

PROCESS DAMPING EFFECT & FRF MODIFICATION

Approved by:

Prof. Dr. Erhan Budak (Thesis Supervisor)

Assist. Prof. Lütfi Taner Tunç (Thesis Co-advisor)

Assoc. Prof. Oğuzhan Yılmaz

Assoc. Prof. Volkan Patoğlu

Assist. Prof. Bekir Bediz

Date of approval   25th July 2017

To my family.

ÇOKLU-MOD SİSTEMLERİ ÜZERİNE BİR ÇALIŞMA:
PROSESS SÖNÜMLEME ETKİSİ & FRF MODIFİKASYONU

Yaser Mohammadi

Üretim Mühendisliği, Yüksek Lisans Tezi, 2017

Tez Danışmanı: Prof. Dr. Erhan Budak

Tez Eş Danışmanı: Yard. Doç. Dr. Lütfi Taner Tunç

ÖZET

Sistemin kararlı davranışın karakteristiklerinin belirlenmesindeki en önemli bilgi Takım tezgâhı sistemlerinden elde edecek dinamik cevaptır. Pek çok çalışmada kolaylık açısından, takım tezgâhı sistemleri genel olarak tekil modlu sistemler olarak ele alınır. Fakat çoklu-mod özellikleri ve bunların çoklu-mod etkilerini hesaba katmak, talaşlı imalat ve ilgili takım tezgâhına yeni dinamik özellikler kazandıracaktır. Bu tez çalışmasında iki adet konu başlığı çoklu-mod sistemleri üzerine çalışılmıştır. İlk olarak, çoklu-mod sistemlerinin freze tezgahı üzerine etkisi proses sönümleme açışından incelenmiştir. Kararlılık lobu diyagramları frekans bazlı çözümlenmiştir ve zaman bazlı yeni bir model kesme takımlarının titreşim davranışını modellemek için geliştirilmiştir. Farklı frekanslardaki modların etkileri kararlılık diyagramlarının ön kısımlarında yer alan düşük kesme hızları için deneysel olarak ispatlandı. Daha sonar, yine bu araştırmanın bir parçası olarak bir yöntem geliştirildi, burada çoklu-mod özelliklerine göre sistemin dinamik davranışı modifiye edildi. Bu yöntemi kullanarak, yapının transfer fonksiyonu modlar arasındaki etkileşimden yararlanılarak modifiye edilebilir. Bir freze takımı için Takım-ucu transfer fonksiyonu bu modele göre baskılanıp istenilen duruma göre ayarlanmıştır ve çekiç testleri ile doğrulaması yapılmıştır.

Anahtar Kelimeler: Çoklu-mod sistemleri, Proses sönümlemesi, Kararlılık lobu diyagramları, Tırlama, FRF modifikasyonu, Modların etkileşimi

ON DYNAMICS OF MULTI-MODE SYSTEMS:

PROCESS DAMPING EFFECT & FRF MODIFICATION

Yaser Mohammadi

Manufacturing Engineering, MSc. Thesis, 2017

Thesis Supervisor: Prof. Dr. Erhan Budak

Thesis Co-advisor: Assist. Prof. Lutfi Taner Tunc

ABSTARCT

Dynamic response of machining systems is the primary information required for determining stability behavior. For the sake of simplicity, machining systems are normally treated as single mode systems in many researches. However, considering multi-mode characteristics and effects of multiple modes introduce new features to machining dynamics. In this thesis, two topics are studied on systems with multiple modes. First, the effect of process damping in multi-mode milling systems is investigated. Stability lobes diagrams are constructed through frequency domain solution and a time domain model is presented to simulate vibrations of the cutting tool. Effects of modes with different frequencies on stability frontier at low speeds are presented and verified experimentally. As the second part of this research, a methodology is developed to modify the dynamic response of structures with respect to their multi-mode characteristics. Using this methodology, the transfer function of a structure can be modified through interaction of structure's modes. Tool-tip transfer function of a milling machine tool is suppressed and verification has been done through hammer impact tests.

Keywords: Multi-mode systems, Process damping, Stability lobes diagram, Chatter, FRF modification, Modes interaction

ACKNOWLEDGMENT

TABLE OF CONTENTS

LIST OF FIGURES

LIST OF TABLES

LIST OF SYMBOLS

k : Structural stiffness

c^s : Structural damping coefficient

c^p : Process damping coefficient

m : mass

N_t : Number of modes

N : Number of cutting teeth

a : Axial cutting depth

ω_c : Chatter frequency

G : Transfer function

$[A_0]$: Directional coefficient matrix

ω_n : Natural frequency

ζ : Damping ratio

T : Tooth passing period

t : time

U : Indentation volume

A : Indentation area

K_{tc} : Tangential cutting force coefficient

K_{rc} : Radial cutting force coefficient

h : Chip thickness

θ : immersion angle

θ_p : Cutter pitch angle

R : Tool radius

β : Helix angle

Ω : Rotational speed

K^d : Indentation coefficient

μ : friction coefficient

q : Modal displacement

φ : Bending rotation angle

E : Young modulus

G' : Shear modulus

I : Cross section area of moment

k' : Shear coefficient

A' : Cross section area of beam element

ρ : Density

L : Beam element length

ω : Excitation frequency

H_{mn} : Receptance function (transverse displacement of point m due to unit harmonic force excitation at point n)

L_{mn} : Receptance function (transverse displacement of point m due to unit harmonic moment excitation at point n)

P_{mn} : Receptance function (bending rotation of point m due to unit harmonic moment excitation at point n)

N_{mn} : Receptance function (bending rotation of point m due to unit harmonic force excitation at point n)

c_y : Translational damping coefficient

c_θ : Rotational damping coefficient

k_y : Translational stiffness

k_θ : Rotational stiffness

γ : Loss factor

Chapter 1 **INTRODUCTION**

Machining industries are permanently required to manufacture parts considering several constraints such as productivity, accuracy and cost in order to fulfill the market demands. Many factors such as cutting techniques, measurements, cutting parameters, etc. contribute to efficiency of machining operations. However, chatter vibration and instability of processes are repeatedly reported to be the main obstacles to achieve those goals [1] because of several negative effects it causes, such as limiting material removal rate (MRR), machine damage, tool wear, poor surface finish, geometrical inaccuracy, increased costs, energy and time lost, etc. Chatter causes increased scrap rate of manufactured parts and tools which leads to huge economic lost. Usually machine tool users are too conservative in selecting the cutting process parameters in order to avoid chatter. Although there have been strong attention to chatter problem in the last decades, it is still on the top of academic and industrial interests in manufacturing research due to demands for higher productivity and efficiency, especially in machining of complex and flexible part (such as thin-walled structures) or hard to cut materials (in aerospace industries).

The primary cause of chatter is the regeneration of waviness of the workpiece surface. A wavy surface is left due to the vibrating tool while cutting. In the next cut, a new wavy surface with a phase difference is generated and, hence, the chip thickness varies, leading to dynamic cutting forces. If the cutting process is in unstable region, the dynamic cutting forces amplify the vibration which causes intensive cutting forces in return. This regenerative mechanism is continued and builds up chatter. Tlusty and Polacek [2] determined the stable cutting depth in orthogonal cutting using cutting force coefficient. Orthogonal stable cutting depth was also calculated by Merrit [3] through Nyquist stability

criterion. In another early work, Tobias [4] studied the regenerative mechanism and represented it as a function of depth of cut and spindle speed using the stability lobe diagrams. Later on, Tlusty [5] presented a stability formulation for end-milling. He adapted the turning formulation to end-milling by taking average number of cutting edges per revolution. Minis and Yanushevsky [6] provided a dynamic milling modelling using Floquet's theorem and determined the stability limits using Nyquist stability criterion. A comprehensive analytical method to predict cutting depth stability in end-milling was proposed by Altintas and Budak [7]. They developed zero-order approximation (ZOA) method by considering only the constant coefficient in the Fourier series expansion of the directional factor in the dynamic formulation and showed its efficiency in obtaining stability lobes in frequency domain. Later, Budak [8] developed the multi-frequency solution to milling stability to improve the chatter predictions in low immersion cutting conditions. It is important to note that most of the studies have been done on prediction of milling stability, the system has been assumed to have a single dominant mode. However, when there are two or more modes with near modal stiffness, the stability limit differs widely from the predicted one using a single mode. Although there are plenty of researches on milling stability, the number of literatures which have included the effect of multiple modes, is limited. Mann et al. [9] employed finite element analysis to study the stability and surface error of a multi-mode milling system. Berglind and Ziegert [10] developed an analytical time-domain model for a turning system with multiple modes. Tang et al. [11] presented a stability prediction method for high-speed finishing end milling considering multi-mode dynamics. In a recent research, Wan et al. [12] studied the milling system stability with multiple dominant modes. It was theoretically proved the stability border for a multi-mode system can be effectively predicted by the lowest envelop of the stability lobes constructed for each single mode separately.

Generally, researchers work on predicting, identifying, avoiding and suppressing chatter. Stability lobe diagram (SLD) is the common tool used to define the border between chatter free region and unstable region, visualized by pair of cutting speed and cutting depth as shown in Figure 1.1. To construct the stability lobe diagram, the frequency response function (FRF) of the system is required. The FRF of a machine tool is affected by the dynamics of all its components; spindle, axes carriage, tool holder, cutting tool, etc. Once

the FRF of the system has been identified, the stability diagram can be predicted for a specific workpiece and cutting parameters.
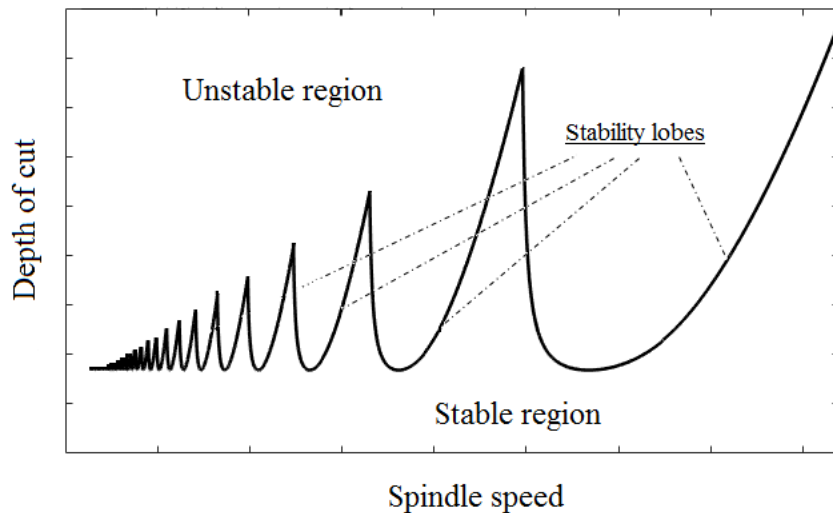
Figure 1.1. A common stability lobes diagram.

The idea is to enlarge the stable region and to compromise the cutting depth and cutting speed which result in maximum material removal rate and enhanced productivity. There are different ways and strategies for these purposes. The first strategy is to take the advantage of lobing effect by proper selecting of cutting parameter combinations (i.e. cutting depth and cutting speed) in the stable region of the SLD. As it can be seen in Figure 1.1, the lobes becomes large at high speeds and high stable cutting depths between the lobes are available which can lead to high MRR, reduced time and cost. The lobing effect can be beneficial at relatively high speeds and is not effective at low speeds, where the lobes get smaller and close to each other. However, there is a phenomenon called process damping which becomes dominant at low speeds. The mechanism of process damping is based on the contact of the flank face of cutting tool and the surface of workpiece which will be discussed in detail later. To benefit from process damping and lobing effects for the purpose improving material removal rate, accurate prediction of stability lobes diagram is essential which indicates the importance of researches on machining vibrations and stability. Constructing the stability lobe diagram and selecting the proper combination of

3

cutting parameters are done before the beginning of machining process. However, there are some online methods as well to prevent chatter during machining. Spindle speed variation is an online technique to disrupt the regenerative effects by varying chatter wave modulation [13]. A similar concept is utilized by using variable pitch cutters and variable helix milling tools in [14, 15].

As mentioned before, the dynamic response of the structure is of great importance in determining the stability frontier. Based on this, many researchers have investigated different ways to passively change the dynamic characteristics of the system for improving the stability limit. This can be done by redesigning and modifying the machine tool structure in order to reduce the flexibility of weak parts and components. However, once the structure is designed and the machine tool is manufactured, the flexible components of the structure can be damped using additional damping devices. Tuned mass dampers are the most common absorbers used to damp the flexible elements of the system. Moreover, active devices such as piezoelectric actuators are also able to improve effectively the stiffness of the weak components, which can be the cutting tool, tool-holder, spindle, or any other component of the machine tool.

As discussed, accurate prediction of stability limit and enlarging the stable zone are among the priorities of machining research field. In this thesis, the focus is on two topics: First, predicting of milling stability limits under effect of process damping and second, enhancing the stability limit by damping the flexible mode of system. Hence, literature reviews on these two topics are given in the following sections, respectively.

1.1 Literature survey on process damping

Even though the proposed methods on predicting stability limit are successful at high cutting speeds, many discrepancies have been reported between predicted stability limit and experimental observations at low cutting speeds. This is mainly due to the effect of process damping which suppresses vibrations at low cutting speeds, leading to increased chatter-free cutting depth as illustrated in Figure 1.2. This effect is crucial for some cases such as

machining of difficult-to-cut materials e.g. nickel alloys and titanium, where on one hand cutting speed is inherently bounded due to low machinability, i.e. tool life issues. On the other hand, cutting depth has to be fixed close to the limits of stability to compensate the reduction of MRR due to low cutting speed.
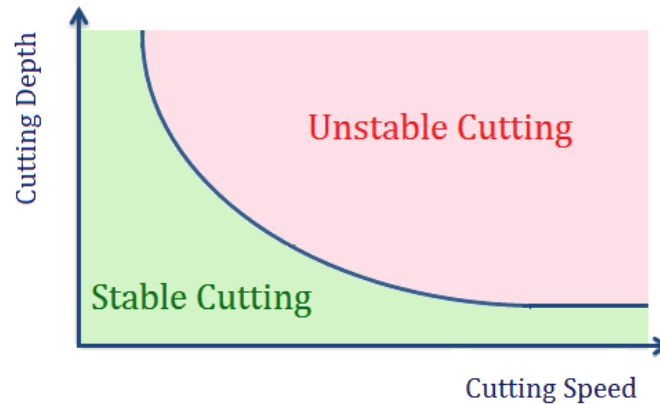
Figure 1.2. Increasing chatter free cutting depth at low speeds.

Although the primary source of damping is known to be structural damping, damping may also be generated due to cutting process itself, which can be much stronger than the structural damping at low speeds. In an early study, Sisson and Kegg [16] tried to find an explanation for chatter behavior at low speeds which was consistent with published experimental observations. They reported that the process stability can be improved by using tools with worn cutting edges and reground flank. Das and Tobias [17] introduced a velocity term into the equations of motion to mimic the process damping effect leading to increased stability limits. However, Tlusty and Ismail [18] showed for the first time that stability frontier arises by decreasing the cutting speed which is caused by periodic contact between the wavy surface and the flank face of tool. Later Wu [19] reported that the indentation of the workpiece material by the tool's flank face is a huge source of damping and developed a model in which process damping effect is described by the indentation forces acting in the tool-workpiece interference. He introduced a ploughing force in normal direction which was related to the amount of displaced material by the tool flank. Assuming an average coefficient of friction, a tangential force was modeled as well.

In [20], Wu's approach was adapted into two degree of freedom milling system. Later, this indentation model was simplified by Chiou and Liang [21] to a piecewise linear viscous damper. This was done by assuming small amplitudes of vibration. However, their model and the latest models based on the vibration amplitudes assumption (Montgomery & Altintas [22], Clancy & Shin [23], Eynian & Altintas [24], etc.) are reliable for the utilized vibration amplitudes and the errors increase in predicting stability limits considering other amplitudes. Ahmadi and Ismail [25] studied the nonlinear effect of process damping in the stability lobes diagram analytically. For this purpose, they used semi-discretization and multi-frequency methods. They developed the linearized model while preserving the vibration amplitude dependence and represent a band of stability between the fully stable and fully unstable regions.

In another early work, Ranganath et al. [26] added the process damping effect to stability of milling by calculating the indentation volume through time domain simulations. Huang and Wang [27] investigated mechanisms of cutting and process damping separately using time domain simulations and worked on peripheral milling stability modeling by developing the cutting force model which included process damping. In another work, Altintas et al. [28] presented a cutting force model including three dynamic cutting force coefficients related to regenerative chip thickness, velocity and acceleration terms. They used Nyquist criterion to solve stability of the dynamic process.

Budak and Tunc [29] proposed an inverse stability method for experimental identification of the additional process damping effect, where the structural damping is deducted from the total damping. They used an energy dissipation principle to relate the process damping to the flank-wave indentation, and identified indentation force coefficients which are then used for estimating the amount of damping force for different cutting conditions and tool geometry [30]. Besides analytical and experimental approaches, Chandiramani [31] proposed a stability model with nonlinear process damping numerically. Furthermore, Jin and Altintas [32] identified the process damping coefficients utilizing the finite element models of micro-milling processes based on material constitutive property. In another identification method [33], the process damping coefficient was predicted from frequency domain decomposition of vibration signal in stable cutting region.

Predicting of stability limit in multi-mode is more complicated than single mode systems, where the tool mode may be the only dominant mode. Some of the researches on stability limit of multi-mode systems were already mentioned. Although there are more researches ([34], [35]) on stability of multi-mode milling systems, they have not considered the effect process damping. On the other hand, the above mentioned researches on process damping have studied single mode systems and considered only the dominant mode for predicting the stability limit. However, the vibrations frequency is one of the most effective parameters in process damping effect [36] which can be very important in the stability behavior of the multi-mode systems. The process damping effect significantly diminishes at low frequency modes as compared to higher frequencies due to the decreased tool-workpiece interaction. Thus, the amount of generated damping by well-separated modes of a system is expected to be different, leading to a different dynamic behavior compared to single mode systems.

1.2. Literature review on modification of system's dynamic response

In machine tools, the dynamic response of the machine tool's structure is mainly responsible for the overall performance of the machine. Among the strategies for avoiding chatter and increasing the stable cutting depth, modifying the dynamic behavior of the structure and damping the flexible mode of the system are among the most practical methods. Optimization of the machine tool structure where the objective is increasing the stiffness of the most flexible part of the structure is of great importance at the design stage. In this regard, topology optimization is widely used to target the eigen-frequencies and flexible modes of the structure [37]. Finite element method (FEM) is a common and strong tool for simulation of structures' flexibility and stability of systems. It makes it possible to simulate and predict the dynamic behavior of the machine tool and its components at the design stage, before construction of the machine [38, 39]. In [40], an approach was presented to predict the machining stability through simulation of chip formation based on FEM. Garitaonandia et al. [41] developed a dynamic model for a grinding machine through finite element analysis. In [42], dynamics of thin-walled workpiece milling was

7

investigated considering variation of dynamic characteristics of the system by the tool position. Apart from FE models, the dynamic response of the system can be predicted analytically using the substructure coupling techniques. Erturk et al. [43] modeled the dynamics of spindle-holder-tool assembly analytically using Timoshenko beam and receptance coupling theories. Through this model, it is possible to simulate the effect of each component on the tool-point FRF and hence, redesigning the components to improve the machine tool's performance against chatter.

In cases where modifying or changing of components is not possible, the stability of system can be improved using vibration control devices which absorb or supply energy. The vibration control systems are mainly divided in two categories based on their operational mechanism; passive and active. Active systems are composed a control feedback system (sensors and controller equipment) and an actuator which applies force to the system based on the feedbacks, in order to counteract and suppress the vibrations caused by flexible elements. Since piezoelectric materials can operate as both sensors and actuators, they are being used in active vibration suppression systems widely and several absorbers have been constructed using them. In [44], embedded piezoelectric elements and shunt circuits were used for chatter reduction in turning. Matsubara et al. [45] successfully suppressed a boring bar using piezoelectric actuators and an inductor-resister (LR) circuit as a mechanical absorber. In [46], an active control system was implemented around the spindle and tool to suppress chatter in milling operation and the stability lobe diagram was actively raised. Browning et al [47] proposed an adaptive vibration control technique using filtered-x least mean square algorithm for reducing chatter in boring bars.

Although active vibration control systems can be very effective and applicable to different excitation conditions, usually they require complicated setup and cost too much. On the other hand, passive devices are less effective and operate in a specified dynamic loading which they tuned for, but they are cheaper, easy to implement and inherently stable despite of active systems. Mechanism of passive devices is based on absorbing the vibration energy of the system. Tuned mass dampers (TMD) are the most used passive devices composed of damping elements and mass. A tuned mass damper was used in [48] to improve the length-to-diameter ratio in boring. Saffury et al. [49] tuned an absorber to damp the vibration of an

external grooving tool. Tarng et al. [50] modified the frequency response function of a turning cutting tool using a tuned vibration absorber which improved the cutting stability. In [51], multiple tuned mass dampers (MTMD) were optimized to improve chatter resistance of machine tools. It was shown that MTMDs have more robustness to uncertainties in dynamic properties of the system compared single TMDs. Wang [52] proposed nonlinear dampers by adding series of friction-spring elements and demonstrate their performance in machining stability improvement. In [53], a frictional damper was introduced to enhance the structural damping in a slender end-mill tool.

1.3. Objectives

The focus of this study is on investigating the dynamic behaviors of systems with multiple modes such as the system shown in Figure 1.3. In this regard, two topics about multi-mode systems have been studied as mentioned in the following two paragraphs:

As previously indicated, the process damping effect is highly influenced by vibration frequency and hence, contribution of multiple modes at distinct natural frequencies (such as modes shown in Figure 1.3) may lead to significant changes in stability of the system as process damping is considered. In this part of the study, the objective was to investigate the effect of process damping in milling with respects to the multi-mode dynamics characteristics of the multi-degree-of-freedom system. For this purpose, different multi-mode systems have been realized on a milling machine tool and the stability limit for multiple modes has been constructed through the frequency domain solution. To have a deeper insight into the dynamics of multi-mode milling and better demonstrate the contribution of modes in the vibration of the tool, a time domain model simultaneously considering multi-mode interaction has been proposed.

In the second part of the study, the focus is on enlarging the stable cutting zones by changing the dynamics of the structure. This can be achieved by increasing the rigidity of flexible components which is done through different approaches in literature as previously discussed. Here, the aspiration was to dampen a flexible mode of a multi-mode system

using the other modes of the system. The same idea of tuned mass dampers has been followed where the vibration modes of the main system and the absorber are close to each other, leading to suppression of the system's dominant mode. In this study, a methodology has been proposed for damping the tool mode (which is usually the most flexible mode in machine tools) by tuning it to the existing modes of the rest of structure.

The outcomes of this study are supposed to be practical guidance for machine tool operators in process planning of cutting parameters, i.e. spindle speeds and depth of cuts, in milling processes which are limited to low cutting speeds and in taking advantage of structure's modes for damping the tool mode and consequently enlarging stable cutting zone.
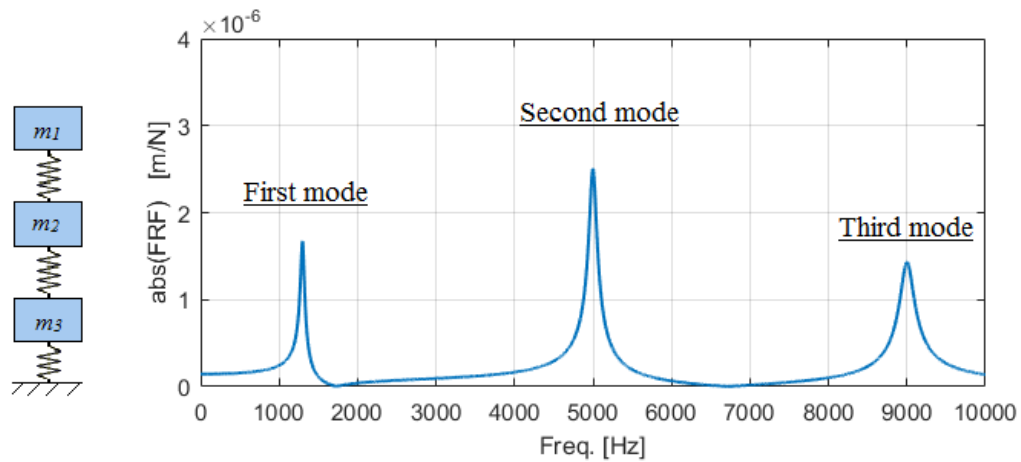
Figure 1.3. An example of a multi-mode system

1.4. Layout of the Thesis

The thesis is organized as follows:

▪ In chapter two, the stability of multi-mode milling system under effect of process damping is studied by constructing the stability lobes diagram. Within this chapter:

- In section 2.1, the frequency domain solution for multi-mode milling stability with process damping is presented and the stability lobes diagram are predicted and contribution of the modes is demonstrated.
- In section 2.2, a time domain model is developed to simulate the vibration behavior of the system at different points of the stability diagram.
- In section 2.3, the experiment setup and cutting tests' results are presented.
- The chapter is concluded in section 2.4.

- In chapter three, the proposed approach to dampen the tool mode is presented. It is shown how to find the proper tool dimensions according to the experimentally obtained FRF of the structure at the tool holder tip. Within this chapter:
  - In section 3.1, the mechanism of vibration absorbers and their function is discussed.
  - In section 3.2 and 3.3, the beam theory and receptance coupling method which are used for FRF predictions are presented.
  - In section 3.4, the method of tool-tip FRF prediction using analytical FRFs of the cutting tool and experimental FRF at the holder tip is given.
  - In section 3.5, the developed procedure of FRF modification and damping of tool mode is discussed.
  - In section 3.6, the simulation results along with experimental results are presented.
  - The chapter is concluded in section 3.7.

- In chapter four, a summary of the thesis is presented which includes the major conclusions of the thesis.

Chapter 2 PROCESS DAMPING EFFECT ON STABILITY OF MULTI-MODE MILLING SYSTEM

In this chapter, the stability of multi-mode milling systems considering process damping is investigated. The effect of different vibration frequencies in such systems are emphasized and it is shown how the rigid modes of a system at low frequencies can change the dynamic response of the system in presence of much more flexible modes. The investigation is done through both frequency domain and time domain analyses. Moreover, experimental investigations are presented as well.

2.1. Dynamics and stability of milling with process damping in frequency domain

The stability of the multi-mode milling system in frequency domain is studied in this section. For this purpose, the analytical frequency domain solution discussed in [8] is used. The multi-mode system is considered as several single mode systems and the stability diagram for each mode is constructed separately. Then, the lowest envelope of the stability limits of all the modes is selected as the ultimate stability limit of the multi-mode system. This approach is valid if the modes of the system are well-separated [12]. In the following subsection, the dynamics of single-mode milling system with the process damping term is briefly presented. The equations of motion of milling system are followed by the frequency domain solution of the stability limits.

2.1.1. Equations of Motion

The cross section of a helical end mill, which is flexible in *x* and *y* directions with *N* number of cutting flutes is illustrated in Figure 2.1. It was mentioned that the multi-mode system is considered as several single mode systems. Thus, the system in Figure 2.1 has one mode is each direction and it is considered as one of the modes in multi-mode system. As the cutter rotates, the cutting tooth indents into the wave left on the cut surface of the workpiece. Correspondingly, an indentation force arises in normal directions on the tool flank face, creating a damping effect. The normal force causes a tangential component as well, assuming a friction coefficient *μ*. For this system, the equations of motion with the effect of process damping can be written in *x* and *y* directions as:

$$
\begin{aligned}
m_{x,i}\ddot{x}_{x,i} + c^t_{x,i}\dot{x}_{x,i} + k_{x,i}x_{x,i} &= F_x; \quad c^t_{x,i} = c^s_{x,i} + c^p_{x,i} \\
m_{y,i}\ddot{y}_{y,i} + c^t_{y,i}\dot{y}_{y,i} + k_{y,i}y_{y,i} &= F_y; \quad c^t_{y,i} = c^s_{y,i} + c^p_{y,i}
\end{aligned}
\qquad i = 1, ..., N_t
\tag{1}
$$

where *m*, c^s and *k* are the modal mass, structural damping, and stiffness of the system, and c^p indicates the average process damping coefficient in each direction, respectively. N_t stands for the number of dominant modes of the system.
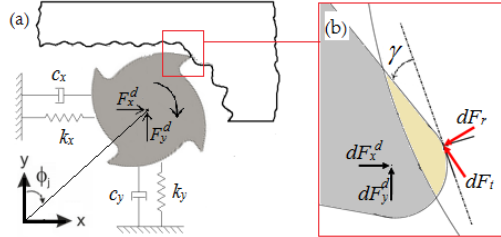
Figure 2.1. Dynamic milling with process damping, (a) cross section of a helical end mill, (b) flank-workpiece interaction

The cutting forces in equation 1 acting on the tool can be written in terms of dynamic displacements and cutting depth [8] as follows:

$$\begin{Bmatrix} F_x \\ F_y \end{Bmatrix} = \frac{1}{2} a K_t \begin{bmatrix} a_{xx} & a_{xy} \\ a_{yx} & a_{yy} \end{bmatrix} \begin{Bmatrix} \Delta x \\ \Delta y \end{Bmatrix} \tag{2}$$

where Δx and Δy are the dynamic displacement of the cutter between the current and previous cutting pass. In the above equation, a_{xx}, a_{xy}, a_{yx} and a_{yy} are the directional coefficients to relate the dynamic forces and dynamic displacements [8].

2.1.2. Milling stability

After writing the dynamic cutting forces in terms of dynamic displacement of cutting tool and mathematical manipulations, the dynamic equation of the system can be written as follows [8]:

$$\{F\} e^{i\omega_c t} = \frac{1}{2} a K_t (1 - e^{-i\omega_c t})[A_0][\mathrm{G}(i\omega_c)]\{F\} e^{i\omega_c t} \tag{3}$$

In the above equations, K_t is tangential force coefficient, $[A_0]$ is the directional coefficient matrix of the milling system and $[G]$ stands for the total transfer function of the system including the effect of process damping;

$$G(i\omega_c) = \frac{1 - r^2 + i2\zeta^t r}{k\left((1 - r^2)^2 + (2\zeta^t r)^2\right)} \quad ; \quad r = \frac{\omega_c}{\omega_n} \quad ; \quad \zeta^t = \zeta^s + \zeta^p \tag{4}$$

where ζ^s and ζ^p are the structural and process damping ratios. The stability of this system can be reduced to an eigenvalue problem [8]:

$$\det[[I] + \Lambda[G_0]] = 0 ; \qquad [G_0] = [G][A_0] \tag{5}$$

14

The eigenvalue Λ in equation 5, is written in terms of process parameters and the chatter frequency ω_c,

$$\Lambda = -\frac{N}{4\pi} K_t a (1 - e^{i\omega_c T})$$ (6)

T is the tooth passing period. Finally, the limiting stable cutting depth can be calculated by rearranging equation 6:

$$a_{\lim} = -\frac{2\pi\Lambda_R}{NK_t}\left(1 + \left(\frac{\Lambda_R}{\Lambda_I}\right)^2\right)$$ (7)

where $\Lambda = -\frac{1}{2a_0}(a_1 \pm \sqrt{a_1^2 - 4a_0})$.

In this solution, a_1 and a_0 are written in terms of the direct transfer functions and the average directional coefficients as detailed in [8]. In order to find the corresponding spindle speed Ω, the below equations are used:

$$\psi = \tan^{-1}\left(\frac{\Lambda_R}{\Lambda_I}\right), \quad \varepsilon = \pi - 2\psi, \quad T = \frac{2k\pi + \varepsilon}{\omega_c}, \quad \Omega = \frac{60}{NT}$$ (8)

2.1.3. Simulation of process damping coefficient

In a previous study [36], the average process damping coefficients were determined through inverse stability solution, assuming that process damping is the only cause for the difference between experimentally obtained stability limit $a_{\lim}^{\exp}$ and analytically calculated stability limit $a_{\lim}^{cal}$, which is verified at high cutting speeds. The experimentally determined process damping coefficients were used to identify the indentation coefficient K^d through damping energy analysis, to simulate process damping coefficients for different cases.

The damping forces arising due to the flank face – workpiece indentation acts against the vibration direction when the tool is moving down the undulation, leading to an additional

15

damping effect (see Figure 2.1) and stabilize the cutting process by dissipating the vibration energy.

The average process damping coefficients, in x and y directions, are defined through energy balance analysis. For such a purpose, the vibration energy dissipated by the average process-damping coefficients is equated to the energy dissipated by the indentation forces over one tool rotation period, T_{sp} as illustrated in Figure 2.2.
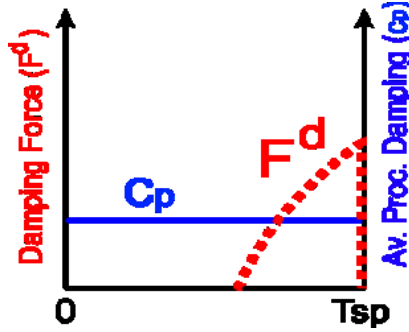
Figure 2.2. Damping energy balance analysis

The additional process damping coefficient at the expected chatter frequency, ω_c is derived as follows:

$$c_i^p = \frac{\int_0^{Tsp} F_i^d(t)\,\dot{\imath}}{\int_0^{Tsp} \dot{\imath}}, \quad i = x, y \tag{9}$$

where, $u = A \sin \omega_c t$

The time varying indentation forces, $F_i^d(t)$, acting on the tool in x, and y directions are calculated by orienting the indentation forces in chip thickness, $F_r^d(t)$, and $F_t^d(t)$, tangential directions, which are written as function of the indentation volume, $U(t)$, and the indentation constant as follow:

$$F_r^d(\mathrm{t}) = K^d U(\mathrm{t})$$
$$F_t^d(\mathrm{t}) = \mu F_r^d(\mathrm{t}) \tag{10}$$

16

In equation 10, $U(t)$ is the indentation volume, which is calculated according to the model given in [36] and μ is the friction coefficient.

2.1.4. Process damping dependence on frequency in multi-mode milling systems

The dynamic milling system consists of several components such as machine tool axis carriers, spindle, tool holder and the cutting tool, each of which introduces dynamic flexibility in a unique frequency range. The vibration frequency significantly affects the process damping as it arises from the indentation between the tool flank face and the undulations left on the workpiece surface. The effect of vibration frequency on the process damping coefficients was previously emphasized by Tunc and Budak [30]. The variation of specific average process damping coefficient with the vibration frequency is shown in Figure 2.3, where it is seen that as the vibration frequency decreases the amount of process damping reduces substantially.
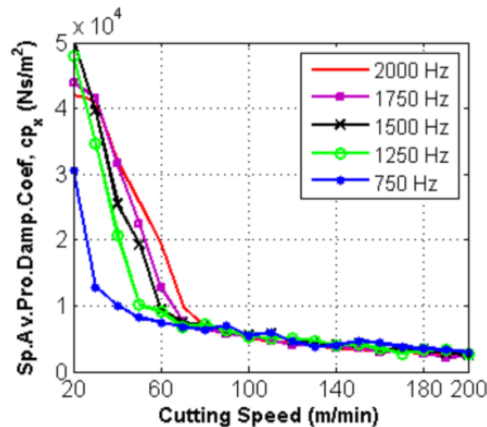
Figure 2.3. Effect of vibration frequency on average process damping coefficients [30]

Figure 2.4 shows how the indentation of the material is more at high frequencies compared to low frequencies, leading to additional damping effect. As the vibration frequency of the cutter decreases, the waves become smoother and their slope decreases.
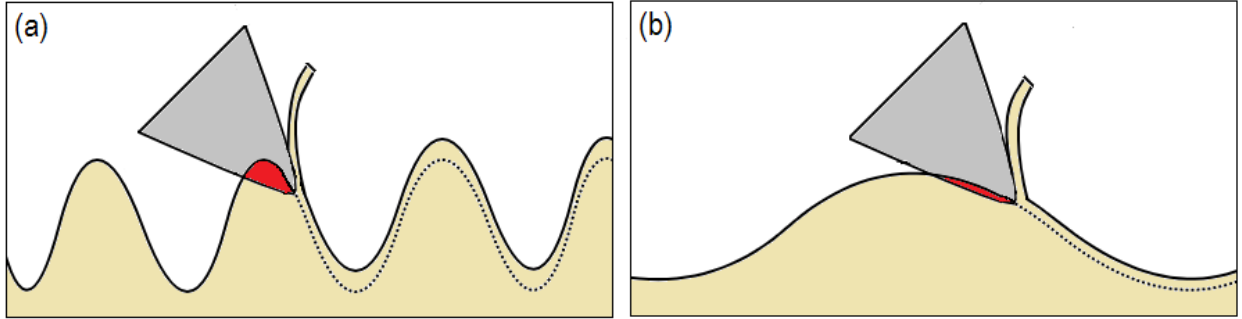
Figure 2.4. Tool-workpiece interference at a) high frequencies b) low frequencies

In dynamic milling, chatter is expected to occur at a single mode. For a milling system having multiple dominant modes at distinct frequencies such as the system shown in Figure 1.3, even though the higher frequency mode is suppressed by process damping, the lower frequency mode may not be suppressed as the process damping is smaller at the lower vibration frequency. Thus, theoretically, the chatter frequency may shift to low or high frequency range depending on the amount of process damping acting on each mode. On the other hand, the vibration frequency dependent process damping may cause the milling system experience higher frequency mode vibration, while it is chattering at lower frequency mode.

2.1.5. Constructing the multi-mode stability lobes with process damping

The amount of process damping acting on a vibrating mode depends on the cutting depth. Thus, the stability limit at a spindle speed can be calculated in an iterative manner as proposed by Tunc and Budak [36]. Although it is a simplification of the nonlinear effect of process damping on stability, within the scope of this study, the stability lobes are calculated separately for each dominant mode with the process damping effect. Then, the lowest envelop of the stability lobes due to all dominant modes is taken as the absolute stability border. However, alternative solution approaches should be further investigated.

A representative stability diagram for down milling of AL7075, including process damping is given in Figure 2.5. For this simulation, half immersion down milling and force cofficients of K_{tc}=1600 MPa and K_{rc}=600 MPa are considered. The tool is an 18 mm diameter, four fluted, solid carbide end mill. The transfer function of the system is shown as

well and as it can be seen there are two dominant modes with almost the same magnitudes which mean the flexibility of the modes are close and comparable.
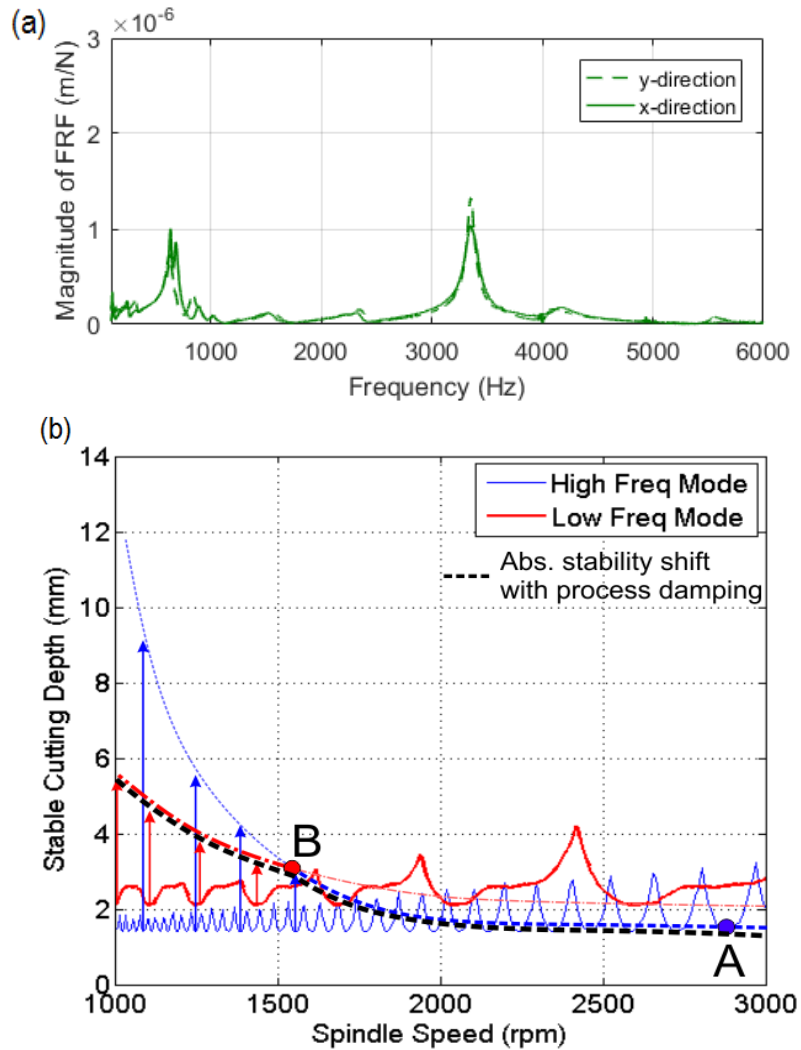
Figure 2.5. Change of the mode governing the absolute stability

The solid lines show the stability lobes due to the two dominant modes, i.e. at low frequency and high frequency, when process damping is ignored. It is seen that, the absolute stability limit is governed by the high frequency mode if the process damping is not considered. However, as the process damping is considered, the absolute stability line of both modes shifts up, where they cross-cut each other at point B. As a result, the high frequency mode governs the absolute stability limit from point A to point B. Then, from point B on, the low frequency mode governs the stability limit. This is due to the fact that,

19

the amount of process damping introduced by the low frequency mode is not enough to increase stability at that vibration frequency. As a result, the absolute stability limit corresponding the low frequency mode fails to shift up as much as the high frequency mode.

The system shown in Figure 2.5 had two dominant modes where their flexibilities were close to each other. However, a more interesting case has been presented in Figure 2.6 for a 14 mm diameter end mill where the flexibilities of the modes are not close and one of them is much more rigid. The mode around 3000 Hz is much more flexible compared to the mode around 700 Hz and its stiffness is almost three times less. If someone calculates the minimum stability limit for these two modes, it can be seen that the minimum stability limit for the low frequency mode is about 2 mm, which is about three times higher than the minimum stability limit of the high frequency mode which is 0.6 mm. For such conditions, many people may decide to consider such a system as a single mode system and ignore the rigid low frequency mode. The stability diagram for this system is shown in Figure 2.6-b. The same cutting conditions as the previous case in Figure 2.5 are considered. The vibration at lower frequency cannot be damped well because of less process damping generated by the low frequency mode. Consequently, the stability limit of the low frequency mode at low speeds is lower than the higher frequency mode and governs the stability limits. This is one of the most important conclusions about multi-mode systems that even though the low frequency mode is much more rigid than the higher-frequency mode and its absolute stability limit without effect of process damping is almost three times higher, the stability limit at low speeds is governed by the low frequency mode.
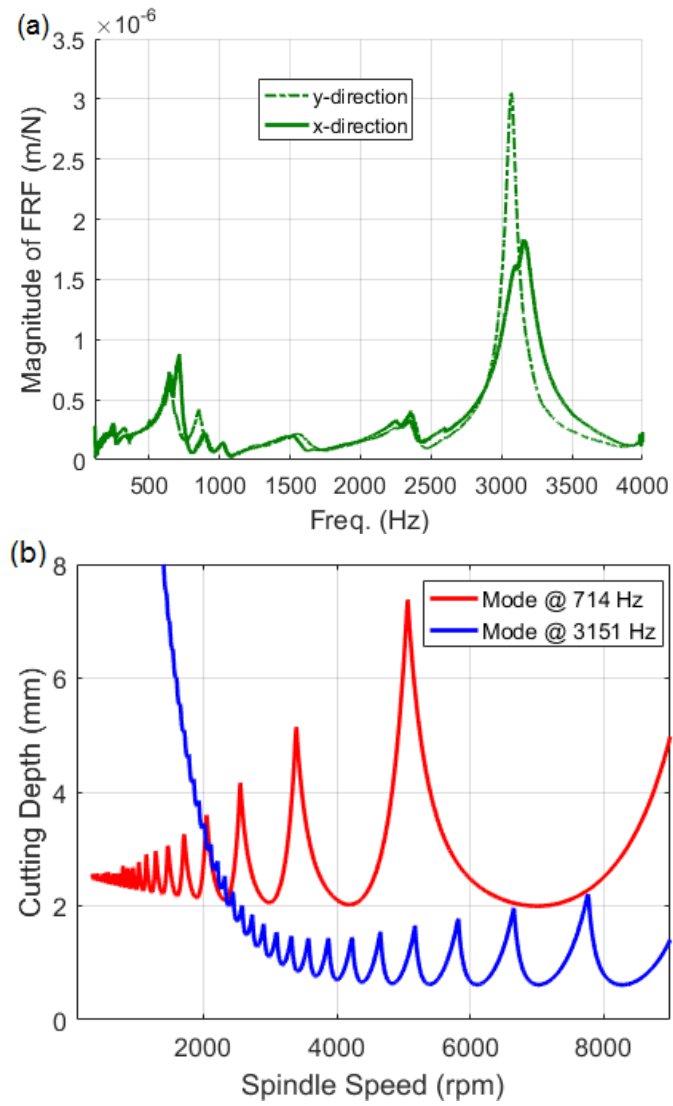
Figure 2.6. a) Frequency response function of milling system with 14mm diameter tool, and b) stability lobes diagram for cutting AL7075

2.2. Time Domain Simulation of Cutter vibration

2.2.1 Mathematical model

A schematic of two DOF milling system with multiple modes in x and y directions is illustrated in Figure 2.7. In order to simplify the dynamics of milling process and concentrate on the multi-modes effect, the workpiece is assumed to be rigid compared to the tool. The tool has N cutting teeth. Assuming that the in-cut tool length is divided in M elements in axial direction (z) with an infinitesimal thickness of dz, the differential cutting forces corresponding to i^{th} element and j^{th} tooth, in the tangential, dF_t, and radial, dF_r, directions (as shown in the cross sectional view of the milling process in Figure 2.7) can be given as:
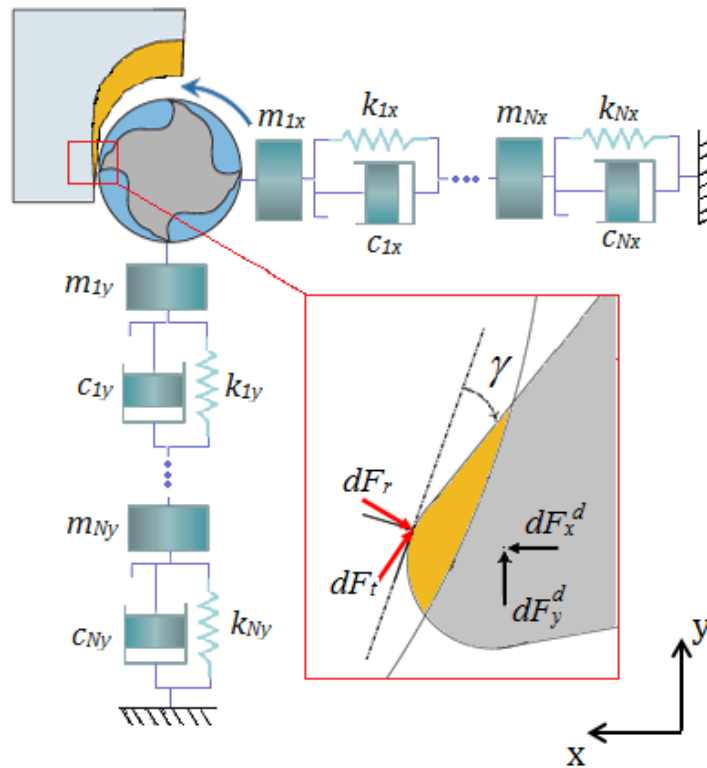
Figure 2.7. a 2-dof multi-mode milling system

$$dF_{t,ij}^{cutting} = K_{tc}h_{ij}\,dz$$

$$dF_{r,ij}^{cutting} = K_{rc}h_{ij}\,dz \tag{11}$$

where K_{tc} and K_{rc} are tangential and radial force coefficients, respectively. h_{ij} is the instantaneous dynamic chip thickness, given as a function of θ_{ij}, the immersion angle measured from the positive y-axis, as follows:

$$h_{ij} = \left[\Delta x \sin \theta_{ij} + \Delta y \cos \theta_{ij}\right] g(\theta_{ij}) \tag{12}$$

$$\theta_{ij} = \Omega t + (j-1)\theta_p - \frac{\tan \beta}{R} i\,dz \tag{13}$$

where

$$\Delta x = x(t) - x(t-T)$$
$$\Delta y = y(t) - y(t-T)$$

Note that Δx and Δy are the total tool deflections, including all the modes, in x and y direction. T is the tooth passing period, R is the tool radius, Ω is rotational speed of the cutter, θ_p is the cutter pitch angle, β is the helix angle of the tool, and the step function g(θij) defines if the corresponding tooth is in cut or not;;

$$g(\theta_{ij}) = \begin{cases} 1, & \theta_{st} \le \theta_{ij} \le \theta_{ex} \\ 0, & otherwise \end{cases} \tag{14}$$

Θ_{st} and θ_{ex} are the start and exit immersion angles of the cutting tooth, respectively. Generally, process damping force is known to be a function of the indentation volume between the flank face and workpiece. Thus, it can be formulated as:

23

$$F_{ij}^{damping} = K_d \, A_{ij} \, dz \tag{15}$$

In the above equation, K_d is the material indentation constant and A_{ij} is the indentation area, which is multiplied by dz to calculate the indentation volume. Once process damping force is added to cutting forces, the total forces in tangential and radial directions are expressed as:

$$
\begin{aligned}
F_{t,ij} &= K_{tc} \, h_{ij} \, dz - F_{ij}^{damping} \\
F_{r,ij} &= K_{rc} \, h_{ij} \, dz - \mu F_{ij}^{damping}
\end{aligned}
\tag{16}
$$

where μ is friction coefficient. By resolving equation 16 the forces in equation in the x and y directions, and summing the forces of all cutting teeth, the total dynamic milling forces with process damping effect acting on the tool can be written as:

$$
\begin{aligned}
F_x &= \sum_{i=1}^{M} \sum_{j=1}^{Nj} \left(-F_{t,ij} \cos \theta_{ij} - F_{r,ij} \sin \theta_{ij} \right) \\
F_y &= \sum_{i=1}^{M} \sum_{j=1}^{Nj} \left(F_{t,ij} \sin \theta_{ij} - F_{r,ij} \cos \theta_{ij} \right)
\end{aligned}
\tag{17}
$$

By substituting equations 15 and 16 in17, the total forces in x and y directions can be formed in a matrix form as follows:

$$
\left\{ \begin{matrix} F_x \\ F_y \end{matrix} \right\} = \begin{bmatrix} H_{xx} & H_{xy} \\ H_{yx} & H_{yy} \end{bmatrix} \left\{ \begin{matrix} \Delta x \\ \Delta y \end{matrix} \right\} = \begin{bmatrix} H_{xx} & H_{xy} \\ H_{yx} & H_{yy} \end{bmatrix} \left\{ \begin{matrix} x(t) - x(t-T) \\ y(t) - y(t-T) \end{matrix} \right\}
\tag{18}
$$

In multiple modes systems, the total motion of the tool can be obtained by summing the modal masses' displacements. Assuming that the modal transformation matrix is normalized to x, the total motion can be obtained such that $x = q_1 + q_2 + \ldots + q_N$, in which q_n $n = 1 : N_t$ are the modal motions of the modal masses for a system with N_t modes. The same

can be applied in y direction. So the total tool motion contains components of each mode, thus the applied force to each mode of the system is dependent on the motions of all the modes. Considering equation 18, the forces can be expressed as:

$$\begin{Bmatrix} F_x \\ F_y \end{Bmatrix} = \begin{bmatrix} H_{xx} & H_{xy} \\ H_{yx} & H_{yy} \end{bmatrix} \begin{Bmatrix} \Delta q_{1x} + \Delta q_{2x} + \ldots + \Delta q_{Nx} \\ \Delta q_{1y} + \Delta q_{2y} + \ldots + \Delta q_{Ny} \end{Bmatrix} \tag{19}$$

where $\Delta q_i = q_i(t) - q_i(t-T)$. In another form:

$$\begin{Bmatrix} F_x \\ \vdots \\ F_x \\ F_y \\ \vdots \\ F_y \end{Bmatrix} = \begin{bmatrix} H_{xx} & \cdots & & & \cdots & \\ \vdots & \ddots & \vdots & \vdots & \ddots & \vdots \\ H_{xx} & \cdots & & & \cdots & \\ H_{yx} & \cdots & & & \cdots & \\ \vdots & \ddots & \vdots & \vdots & \ddots & \vdots \\ H_{yx} & \cdots & & & \cdots & \end{bmatrix}_{2N \times 2N} \begin{Bmatrix} q_{1x}(t) - q_{1x}(t-T) \\ \vdots \\ q_{Nx}(t) - q_{Nx}(t-T) \\ q_{1y}(t) - q_{1y}(t-T) \\ \vdots \\ q_{Ny}(t) - q_{Ny}(t-T) \end{Bmatrix}_{2N \times 1} \tag{20}$$

As discussed above, the applied force to each mode results from the motions of all the modes. This dependency of the forces couples the equations of the modal systems in each direction:

$$\begin{cases} m_{q_{nx}} \ddot{q}_{nx} + c_{q_{nx}} \dot{q}_{nx} + k_{q_{nx}} q_{nx} = F_x \\ m_{q_{ny}} \ddot{q}_{ny} + c_{q_{ny}} \dot{q}_{ny} + k_{q_{ny}} q_{ny} = F_y \end{cases} \quad ; \quad n = 1 : N_t \tag{21}$$

where m_q, c_q and k_q are the modal mass, modal stiffness and modal damping of the modes of the system. Finally, the motion equation of cutting tool considering the effects process damping and multiple modes can be represented in the x and y directions as follows:

$$[M_q]\{\ddot{Q}(t)\} + [C_q]\{\dot{Q}(t)\} + [K_q]\{Q(t)\} = \{F\} \tag{22}$$

with

$$[M_q] = diag\,(m_{q_{1x}},...,m_{q_{Nx}},m_{q_{1y}},...,m_{q_{Ny}})$$

$$[C_q] = diag\,(c_{q_{1x}},...,c_{q_{Nx}},c_{q_{1y}},...,c_{q_{Ny}})$$

$$[K_q] = diag\,(k_{q_{1x}},...,k_{q_{Nx}},k_{q_{1y}},...,k_{q_{Ny}})$$

$$\{Q(t)\} = \left[q_{1x},...,q_{Nx},q_{1y},...,q_{Ny}\right]^T_{1\times 2N}$$

$$\{F\} = \left[F_x,....,F_x,F_y,...,F_Y\right]^T_{1\times 2N}$$

In the above representations, 'diag' signifies a diagonal matrix. Substituting the cutting forces described in equation 20 into equation of motion yields:

$$[M_q]\{\ddot{Q}(t)\} + [C_q]\{\dot{Q}(t)\} + [K_q]\{Q(t)\} = [H]\{Q(t)\} - [H]\{Q(t-\tau)\} \tag{23}$$

The first-order representation of the above equation can be expressed by defining the state variable *R(t)* in terms of the modal positions and velocities,

$$\{R(t)\} = \left[\{Q(t)\},\{\dot{Q}(t)\}\right]^T \tag{24}$$

$$\begin{bmatrix} O & M_q \\ I & O \end{bmatrix}\{\dot{R}(t)\} + \left(\begin{bmatrix} O & C_q \\ O & -I \end{bmatrix} + \begin{bmatrix} O & K_q \\ O & O \end{bmatrix} - \begin{bmatrix} H & O \\ O & O \end{bmatrix}\right)\{R(t)\} = \begin{bmatrix} H & O \\ O & O \end{bmatrix}\{R(t-T)\} \tag{25}$$

where $I_{2N\times 2N}$ and $O_{2N\times 2N}$ are identity and zero matrices, respectively. The first-order equation 25 is solved by classic 4th order Runge-Kutta method to illustrate the vibration of the multi-mode system with effect of process damping.

2.2.2 Simulation results

Simulations results for the system Figure 2.6 is shown in presented in Figure 2.8. The spindle speed is 1000 rpm and the cutting depth is 1.5 mm. As predicted in Figure 2.8, the system is stable and the vibration amplitude is not increasing. The vibration spectrum which is given in Figure 2.8-b reveals that both modes have been excited. However, the amplitude at the second mode is higher which was expected since this mode is more flexible. The cutting and damping forces are presented in Figure 2.8-c and Figure 2.8-d. From the displacement and damping force figures, it can be concluded that as the amplitude is growing up, the amount of generated damping force is also increasing and damp the vibration until it stabilize the cutting process and the vibration amplitude stays constant.
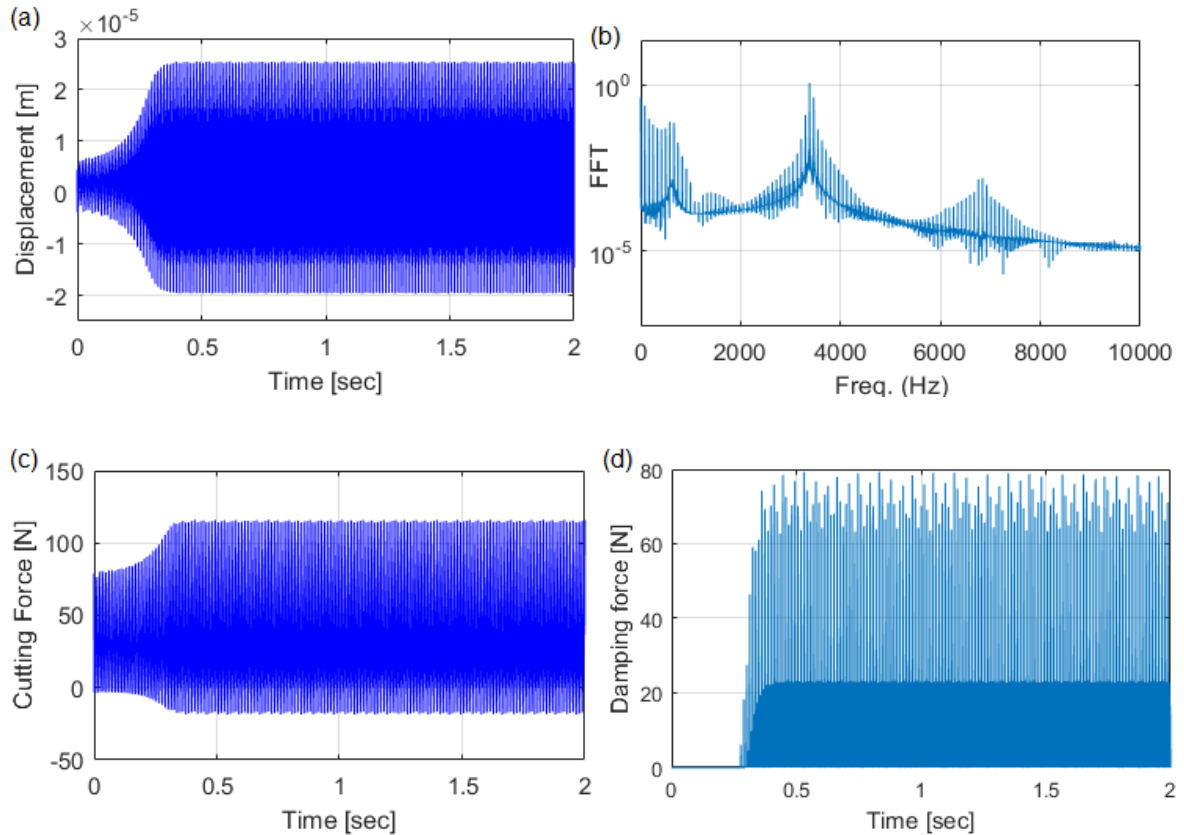
Figure 2.8. Simulation results for cutting AL7075 at 1000 rpm with a 14 mm diameter endmill. a) displacement, b) frequenct spectrum of displacement, c) cutting force, d) damping force, (in y direction).

Two chatter cases have been simulated in Figure 2.9 at two different cutting speeds. The cutting speed in Figure 2.9-a and -b is 1000 rpm, the same speed as in Figure 2.8, but the cutting depth is 3 mm which is in the unstable region according to Figure 2.6. As it can be seen, chatter has completely developed and the system is unstable. But note that even though at the stable cutting depth the second mode was dominant (look at Figure 2.8-b), the spectrum in Figure 2.9-b reveals that chatter has occurred due to the first mode, i.e. the low-frequency mode which has failed to damp its vibration. The second case is at 4834 rpm with the cutting depth of 1 mm. Despite the previous case, Figure 2.9-d indicates that chatter has developed at the second mode, i.e. the high-frequency mode. This verifies the claim that the chatter can develop at both modes depending on the cutting speed and it shifts from the low frequency mode to the high frequency mode as cutting speed increases.
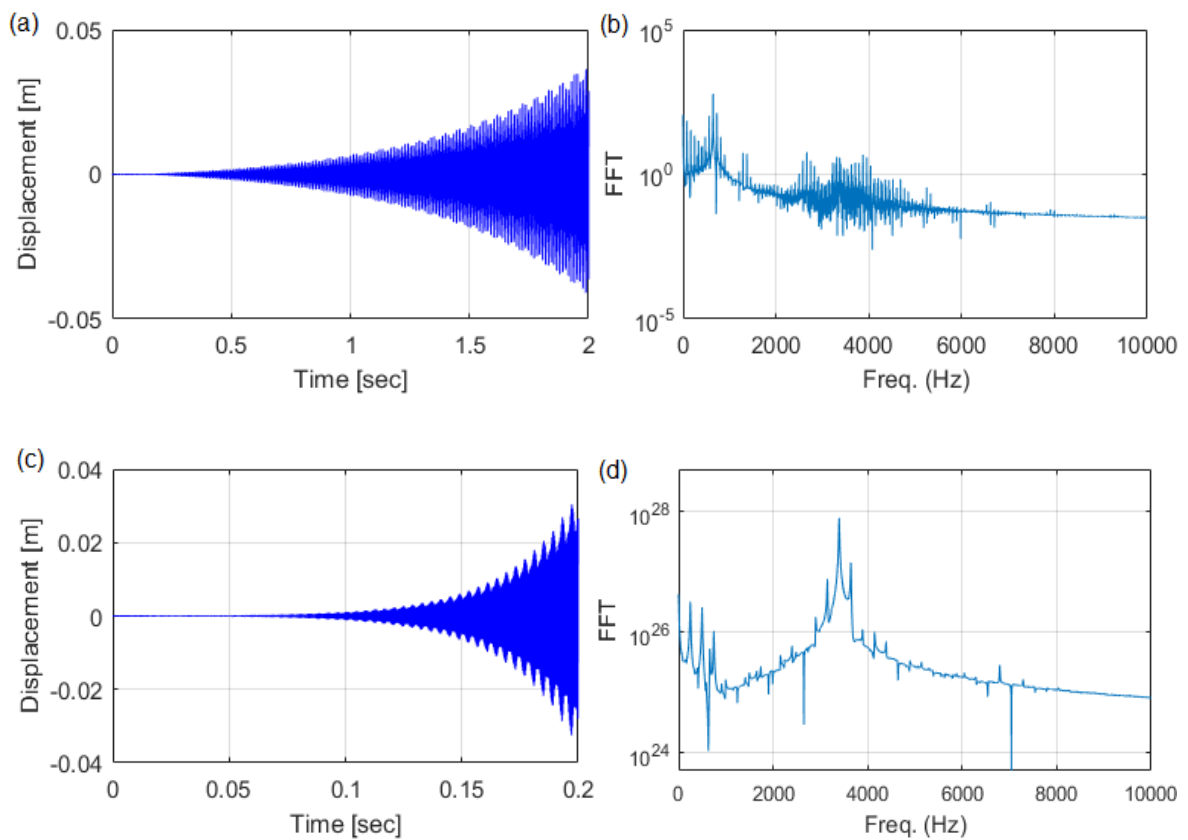
Figure 2.9. Displacement and frequency spectrum in unstable region at a,b) 1000 rpm and c,d) 4834 rpm for the same system of Figure 2.8.

2.3. Experimental investigation

In this section, the effect of process damping on the dynamics of the multi-mode milling system is experimentally investigated to verify the simulation results given in the previous section. Two cases have been considered on a five-axis milling machine tool with two different tools and materials; case one: an 18 mm diameter end mill cutting AISI1050, and case two: an 12 mm diameter end mill cutting AL7075. Both tools are carbide end-mills with four cutting flutes. They were clamped to the spindle-holder assembly with the overhang length is 60 mm for both cases. All the experiments were conducted on DECKEL MAHO 5-axis milling center and the tool holder SK40 ER32C 160G has been used.

2.3.1. FRF measurements

The frequency response functions (FRFs) of both cases have been measured and they are shown in Figure 2.10. The modal parameters of both cases are also given Table 1 and Table 2. It can be seen that there is a dominant mode which is much more flexible compared to others. Many may consider such cases as a single mode system and ignore the low-magnitude modes around 700 Hz. However, it is verified experimentally in this section that how important and determinative the effect of such modes can be.
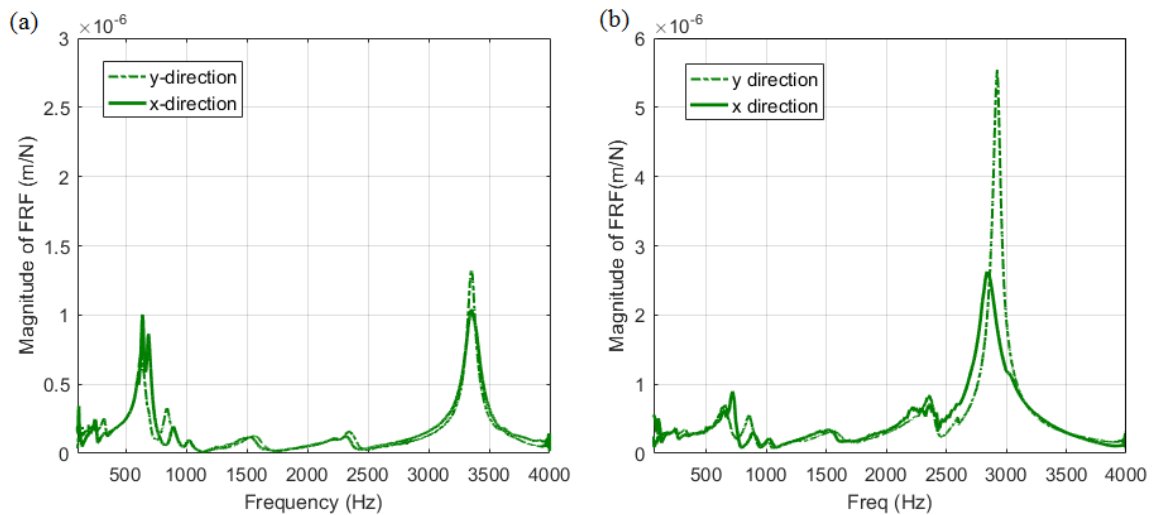
Figure 2.10. Frequency responses function of a) case 1, and b) case 2.

Table 1. Modal parameters for the system case 1.

	k_x (N/m)	f_x (Hz)	ζ_x (%)	k_y (N/m)	f_y(Hz)	ζ_y(%)
1st mode	4.6e7	636	1.8	2.0e7	634	5.4
2nd mode	3.4e7	3352	1.5	4.4e7	3353	1.1

Table 2. Modal parameters for the system case 2.

	k_x (N/m)	f_x (Hz)	ζ_x (%)	k_y (N/m)	f_y(Hz)	ζ_y(%)
1st mode	1.8e7	712	3.1	1.6e7	653	5.4
2nd mode	1.0e7	3151	2.8	1.4e7	3065	1.2

3.3.2. Cutting tests conditions

In the cutting tests the spindle speeds are selected such that the effect of process damping on the absolute stability due to both modes can be observed. The cutting test conditions are given in Table 3 and Table 4 for first and second cases, respectively. The feed rate was set to 0.05 mm/rev/tooth and the radial immersion was 50%, i.e. half immersion. In none of the tests coolant was used and all of them were in dry-cutting condition.

Table 3. Cutting tests conditions for case 1.

Test number	Spindle speed (rpm)	Cutting speed (m/min)
1	3730	211
2	2585	146
3	2060	116
4	1245	70
5	895	51
6	540	31

Table 4. Cutting tests conditions for case 2.

Test number	Spindle speed (rpm)	Cutting speed (m/min)
1	5181	195
2	3531	133
3	2531	95
4	2071	78
5	1411	53
6	1011	38

2.3.3. Designed workpiece for experiments

In order to perform the cutting tests effectively and save more time, the workpiece part was designed as a staggered part with steps as shown in Figure 2.11. The steps' increment was 1/2 of the absolute stability limit. Thus, the cutting depth could be increases gradually and capture the stability limit accurately. The length of each step was selected as 1.2 times of the tool diameter. So enough time could be provided for chatter to be developed. After each cutting level, the machine was stopped to let the tool stabilize before the next cutting level. This way it was insured that the vibrations of previous steps don't affect the vibrations while cutting the next step.
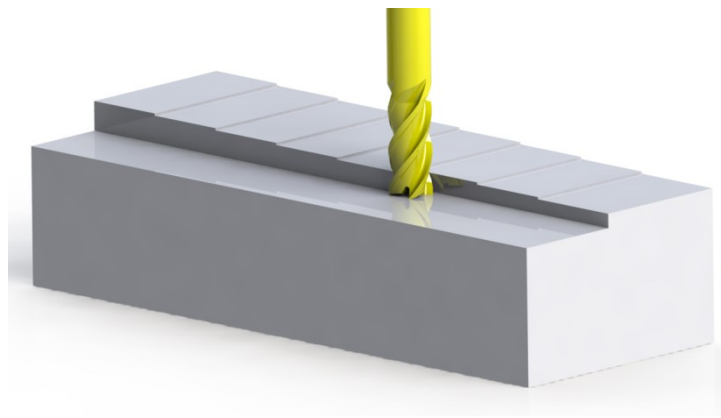
Figure 2.11. The workpiece with steps used for the cutting tests.

2.3.4. Chatter detection method

The experiment setup is shown in Figure 2.12. Compared to turning, realizing chatter in milling can be more difficult and challenging especially for more complicated multi-mode systems. In this work, different data have been collected for the purpose of identifying chatter and the corresponding chatter frequency, ω_c: vibration spectrum, sound spectrum and surface photo. The chatter detection methods are illustrated in Figure 2.13 and Figure 2.14. Examining the workpiece surface after cutting can be very helpful for recognizing the stability limit since chatter deteriorates the cut surface and the feed marks, which can be seen in stable region, cannot be identified easily in unstable region. However, to recognize the corresponding chatter frequency, ω_c, vibration or sound data are required. Relying on one type of data can be problematic since it may doesn't capture ω_c. As chatter happens, the system starts vibrating at the corresponding frequency ω_c, and spectrum magnitude increases around the vibrating mode. This data has been collected using an accelerometer attached to the spindle tip (look at Figure 2.12). A directional microphone is also used to record the chatter sound and to capture the spikes around ω_c.
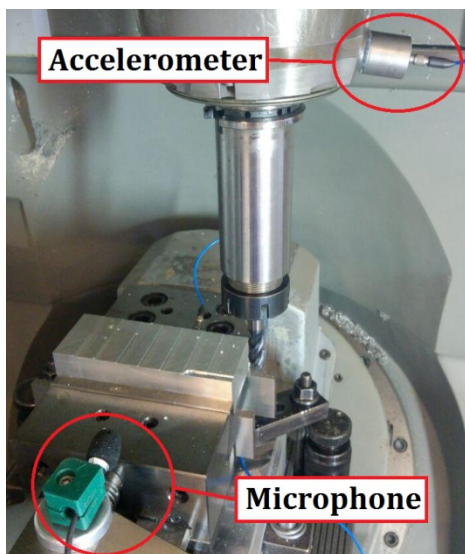
Figure 2.12. Experiment setup
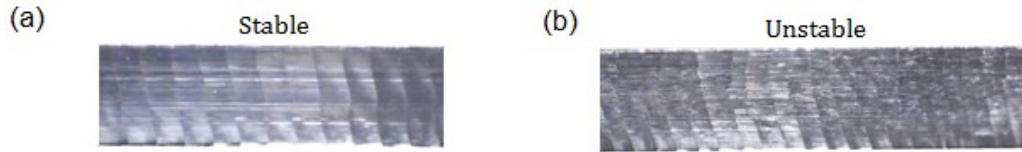
Figure 2.13. a) cut surface in stable region, b) cut surface in unstable region.
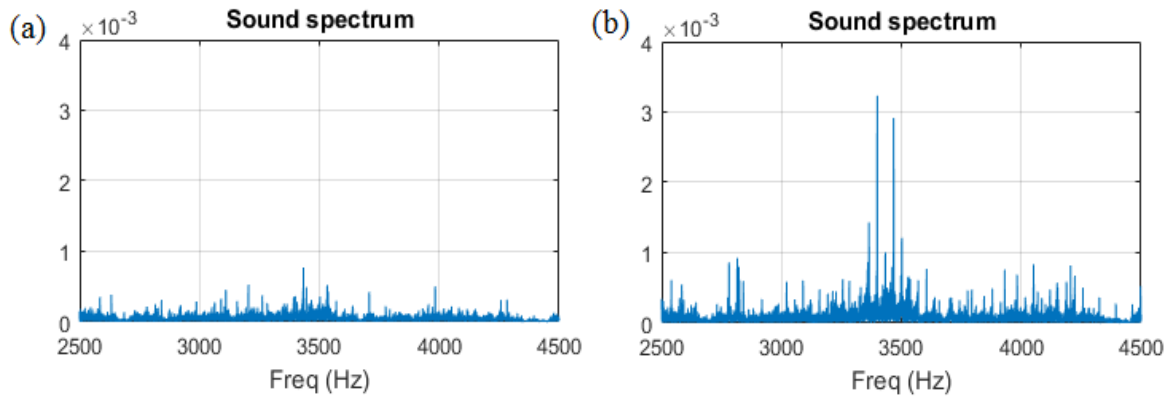
Figure 2.14. Chatter detection through sound spectrum, a) cutting in stable zone b) cutting in unstable zone

2.3.5. Experimental results

The stability diagrams with results of the cutting tests are shown in Figure 2.15. As it can be seen, the experimental results have good agreement with the simulated stability limits. At the process damping speeds, although the most flexible mode generates large ploughing forces and offers high stability limits, chatter has happened at very lower cutting depths. Note that absolute stable depth of cut without considering process damping for the first mode is more than twice of the absolute stable cutting depth of the second mode. It is the most interesting aspect of multi-mode systems that the modes with almost half of the measured structural stiffness of other modes can govern the stability limits at process damping speeds. This verifies the fact mentioned in [30] that the process damping is highly influenced by vibration frequency. In Figure 2.16 and Figure 2.17, the spindle vibration spectrum and the sound spectrum for two different spindle speeds are shown. The green lines show the harmonics tooth passing frequencies. From Figure 2.16 it is clearly seen that the chatter has been developed at the second mode of the system at 5181 rpm. However, as

33

the spindle speed is decreased to 1011 rpm, the chatter mode shifts to the first mode, which is shown in Figure 2.17. Note the in Figure 2.16 the spectrum doesn't show any increase in magnitude around the first mode which means this mode is not responsible for the developed chatter, while in Figure 2.17 the second mode has been damped and no spikes can be seen in this frequency range.
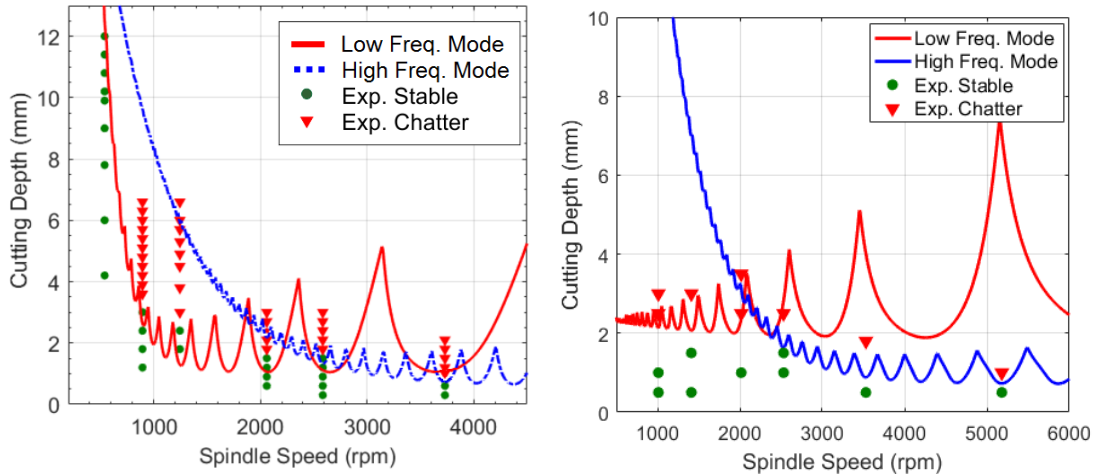
Figure 2.15. The stability lobes diagrams and cutting test results for a) case 1 and b) case 2.
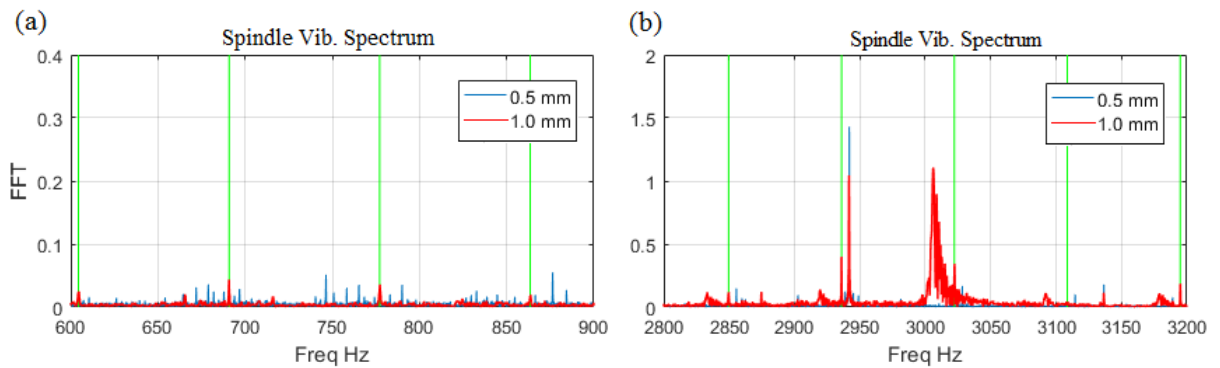
Figure 2.16. Chatter at second mode; spindle vibration spectrum (case 1) at 5181 rpm, a) low frequency range b) high frequency range

34
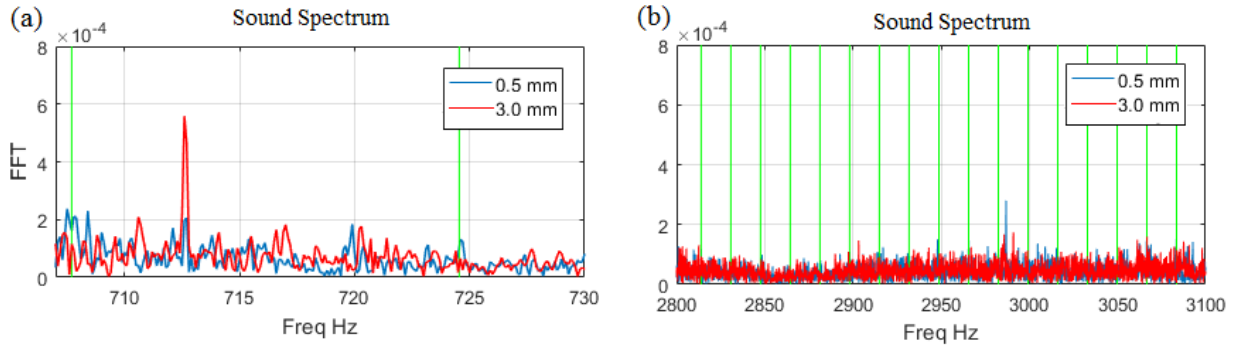
Figure 2.17 Chatter at first mode; spindle vibration spectrum (case 1) at 1011 rpm, a) low frequency range b) high frequency range

2.4 Conclusion

In this chapter, the process damping effect on stability limit of milling systems with multiple modes was investigated. To the author's knowledge, the previous studies concerning process damping have studied its effect on stability of single mode systems and have ignored the other modes. However, process damping is highly influenced by chatter frequency, according to the modes of the milling system. In the presented thesis, process damping effect was investigated for a multi-mode milling system. The theoretical simulations were done in both frequency domain and time domain and they verified by cutting experiments. The effect of process damping on the responsible chatter modes was demonstrated. In general, the absolute stability limit is expected to be governed by the most flexible mode. However, it was shown that under the effect of process damping, the mode governing the absolute stability may shift to other modes at lower frequencies even if their rigidities are much more than the most flexible mode of the system at the higher frequencies. In a certain cutting speed zone, due to the high process damping caused by the high-frequency modes of the milling system, chatter may develop at the low-frequency modes at a depth of cut lower than the predicted one considering only the high frequency mode. Thus, the region which was expected to be stable with the assumption of single mode system at low cutting speeds is no more stable and chatter can develop due to the vibrations of the rigid low frequency mode. This shows the importance of considering

35

multiple modes when determining the stability limit, even if one of the modes is dominant and much more flexible than the others. This is mainly due to the fact that the amount of process damping generated by low frequency modes is not enough to stabilize the process. The high frequency mode makes waves on the workpiece surface with shorter length and higher slopes, leading to higher process damping effects and consequently higher stability limit. Such information may be used to identify the cross cutting point, where the mode governing the absolute stability shifts from high frequency mode to the low frequency mode with the effect of process damping. Such a point would show the cutting speed after which the absolute stability limit may not further increase with decreasing cutting speed.

For better understanding the stability diagram of a multi-mode milling system, consider the schematically illustrated stability diagram in Figure 2.18. At a certain cutting speed, $V_{cutting}$, by increasing the depth of cut gradually from point zero to point B, the system experiences five different vibrating behaviours. In the first region, none of the modes are excited and the system is fully-stable. By increasing the cutting depth and entering the second region, the flexible high-frequency mode excites and starts vibrating. However, this vibration causes generating process damping forces which in turn damp the vibration. This leads to limit cycle oscillations of the system at this mode and the amplitude of the vibration remains almost constant. As the cutting depth goes to region 3, the other mode also excites, but it is damped as well due to the process damping effect and cutting in this region is stable, even though it is vibrating at both modes. But as the cutting depth is crossing from region 3 to region 4, the amount of process damping generated by the low frequency mode is no more enough to stabilize its vibration which leads to developing chatter at this mode and system becomes unstable, even though the high frequency mode is still producing enough damping to damp itself and prevent chatter to be developed. Finally in region 5, chatter can be developed at both modes resulting in fully-unstable conditions.
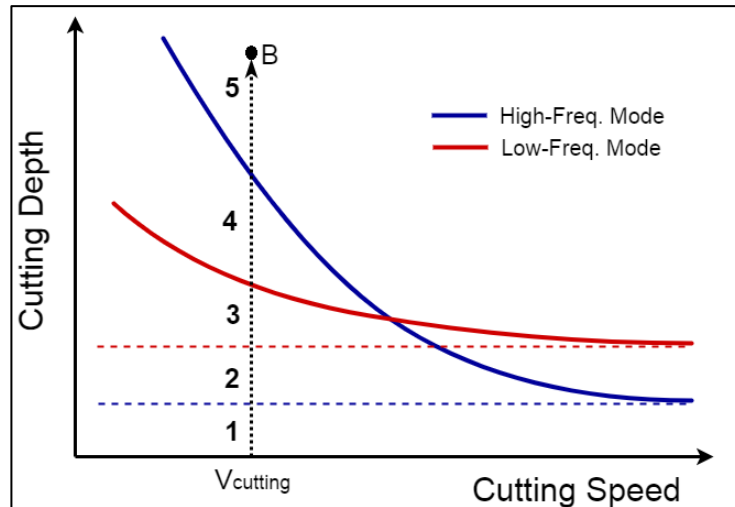
Figure 2.18. Schematic of stability lobes diagram for a multi-mode system

The experimental results showed that the absolute stability limit may be governed by the low frequency modes rather than the high frequency modes at low cutting speeds with the effect of process damping. Under such circumstances if the amount of process damping introduced by the lower frequency mode is not enough to stabilize chatter vibration at that mode, it will limit the chatter-free material removal rate, leading to less productivity. This may be considered as a typical case when a heavy duty milling operation is aimed to be performed at a machine tool with flexible column, axis carriages, spindle or tool holder, which introduces relatively low frequency modes. The resulting stability diagram indicates that the low frequency mode must not be ignored even if it is too rigid compared to the high frequency mode and considering only the most dominant mode of the system may confuse the machine users as they encounter chatter at cutting depths which were expected to be stable.

37

Chapter 3 TOOL-TIP FRF MODIFICATION USING MULTI-MODE CHARACTERISTICS OF STRUCTURE

As discussed in the first chapter, the primary information required for constructing the stability lobe diagram is the frequency response function of the system, including the machine tool's body, spindle, tool holder and cutting tool. The stability border of a system is hugely influenced by its dynamic characteristics where high flexibility of the system can drastically decrease the process stability. Therefore, one of the machine tool manufactures' objectives is to increase the rigidity of the system which results in less vibrations, enlarged stable cutting zone and consequently increased material removal rate. To achieve this goal, there are several approaches to damp the flexible modes of the system, including implementing vibration absorbers, as discussed in the first chapter. In this thesis, a different approach is followed in which the flexible tool's mode is damped without using any external devices, but by the modes of the machine tool structure itself. In this regard, the tool is tuned in such a way that its natural frequency is the close to one of the natural frequencies of the rest of the structure, i.e. the FRF of the system at the tool-holder tip. This is similar to the idea of tuned mass dampers where the modal parameters of the system and the absorber are tuned to each other. The FRF of the tool which is obtained through beam analysis is coupled to the systems FRF at the holder tip to obtain the overall FRF of the system.

This chapter is organized as follows: The mechanism of tuned mass dampers is briefly discussed in section 3-1. Then, the Timoshenko beam theory which is used for the beam analysis and obtaining the dynamic response of the tool is presented in section 3-2. It is followed by section 3-3 which contains the receptance coupling method. Then, in sections

3-4 and 3-5 the tool tip FRF prediction method used in this thesis and the developed methodology of tuning the tool dimensions and damping the tool mode are discussed. Finally, the simulation results along with experimental results are presented in section 3-6 and the chapter is concluded in section 3-7.

3.1. Generalities about vibration absorbers

Tuned mass dampers (TMD) or dynamic vibration absorbers (DVA) are widely used to suppress vibrations and protect structures from damage and structural failure. Indeed, the TMD absorb the vibrating energy of the main system leading to suppressed vibrations of the system. A typical TMD, consist of a mass (m), spring (k) and damping (c) elements, is attached to the system as shown in Figure 3.1. The mass, stiffness and structural damping of the main system are shown as m_s, k_s and c_s, respectively.
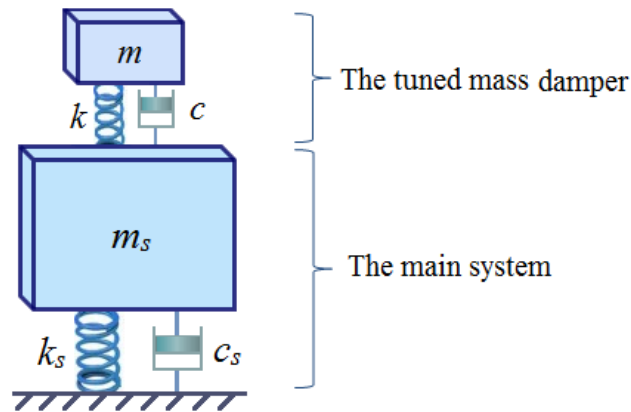
Figure 3.1. A typical tuned mass damper (TMD) attached to a system.

Applying a harmonic force $F(t)$ on the system, the equations of motion can be written as:

$$m \ddot{} \qquad \dot{} \quad \dot{} \qquad -x_s) = 0$$
$$m_s \ddot{} \qquad \dot{} \qquad \dot{} \qquad \dot{} \qquad x) = F(t) \tag{26}$$

where $F(t)=F_0 e^{i\omega t}$. Thus the response of the system is in the same form as $x_s(t)=X_s e^{i\omega t}$. Rearranging the equation of motions, the transfer function between the displacement of the system and the applied force can be obtained as:

39

$$\frac{X_s}{F_0} = \frac{k - m\omega^2 + ic\omega}{\left(k_s - m_s\omega^2 + ic_s\omega + k + ic\omega\right)\left(k - m\omega^2 + ic\omega\right) - \left(k + ic\omega\right)^2} \qquad (27)$$

In general vibration problems, the objective is to minimize the displacement of system which means to minimize the peak of the transfer function in equation 27. For this purpose, the modal parameters of the absorber, i.e. the mass, stiffness and damping, have to be optimized. In [54], the optimum parameters which cause minimum magnitude of transfer function were analytically determined by Den Hartog. The optimized TMD splits the main system's mode into two smaller modes with equal magnitude peaks. However, for chatter problem application, equal peaks cannot be the optimal solution since the critical stability limit is inversely proportional to negative real part of the transfer function. Later, Sims [55] found the optimal parameters for chatter problem in turning which lead equal troughs in the real part of transfer function. The performance of TMDs with both equal peaks and equal real troughs approaches are illustrated in Figure 3.2 through the corresponding optimal transfer functions. As it can be seen, the peak of transfer function has been divided to two smaller peaks at right and left side of the system's natural frequency according to the equal peaks approach. However, based on the equal real troughs approach, the magnitude of the transfer function is higher but the negative real part has been improved. The amount of damping depends on the mass ratio of the system and the absorber, m/m_s, which is usually limited due to the physical constraints. In practice, normally the allowable mass ratio cannot be higher than 0.05.
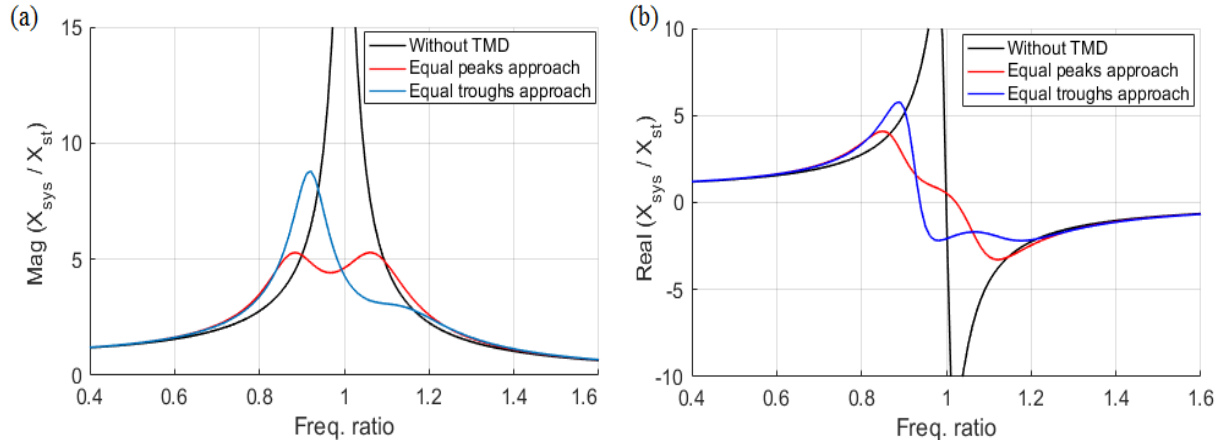
Figure 3.2. Transfer function of a system with and without TMD, a) magnitude b) real part of FRF.

3.2. Beam analysis

There are different theories for describing the dynamic behavior of a beam, such as Euler Bernoulli beam, Rayleigh beam and Timoshenko beam theories. The latter one is used in this thesis since it is found to be most accurate theory for thick beams with low length to diameter ratios since it takes into account the effect of shear deformations as well as rotary inertia which are neglected in Euler Bernoulli beam theory. Figure 3.3 shows a deformed Timoshenko beam element where y is the lateral displacement and φ is the bending rotation angle.
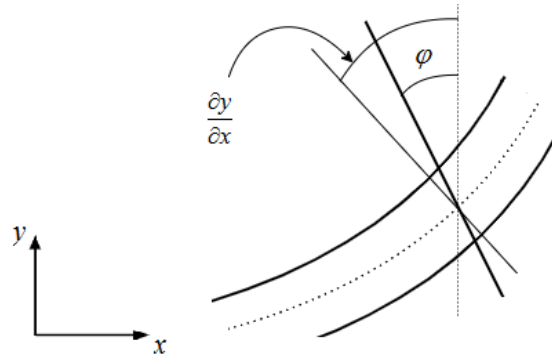
Figure 3.3. A deformed Timoshenko beam element

The governing differential equations of the beam element shown in Figure 3.3 after mathematical manipulations can be presented in uncoupled form as follows [56]:

$$\frac{\partial^4 y(x,t)}{\partial x^4} - \rho\left(\frac{E+k'G'}{k'EG'}\right)\frac{\partial^4 y(x,t)}{\partial x^2 \partial t^2} + \frac{\rho A'}{EI}\frac{\partial^2 y(x,t)}{\partial t^2} + \frac{\rho^2}{k'EG'}\frac{\partial^4 y(x,t)}{\partial t^4} = 0 \tag{28}$$

$$\frac{\partial^4 \varphi(x,t)}{\partial x^4} - \rho\left(\frac{E+k'G'}{k'EG'}\right)\frac{\partial^4 \varphi(x,t)}{\partial x^2 \partial t^2} + \frac{\rho A}{EI}\frac{\partial^2 \varphi(x,t)}{\partial t^2} + \frac{\rho^2}{k'EG'}\frac{\partial^4 \varphi(x,t)}{\partial t^4} = 0 \tag{29}$$

In the above equations, E is young modulus, k' is shear coefficient, G is shear modulus, ρ is density, A' is cross section area of the beam element, and I is cross-sectional area moment of inertia. To solve the above equations and obtain the solution of the eigenvalue problem, both end conditions of the beam are considered to be free since the free-free beam element can be later coupled to other elements and free boundaries can be modified and converted to other conditions easily by structural modifications. Free boundaries imply both shear force and moment at the ends to be zero. Assuming harmonic behavior,

$$y(x,t) = \tilde{\ } \qquad \varphi(x,t) = \tilde{\zeta} \tag{30}$$

the partial differential equations (28) and (29) can be converted to ordinary differential equations in frequency domain. In [56], the characteristic equation for such a free-free beam was obtained as:

$$\begin{vmatrix} D_{11} & D_{12} \\ D_{21} & D_{22} \end{vmatrix} = D_{11}D_{22} - D_{12}D_{21} = 0 \tag{31}$$

where

$$D_{11} = (\alpha - \lambda)(\cos\alpha - \cosh\beta)$$

$$D_{12} = (\lambda - \alpha) \sin \alpha + \frac{\lambda \alpha}{\beta \delta}(\beta - \delta)\sin \beta$$

$$D_{21} = -\lambda \alpha \sin \alpha + \frac{\alpha - \lambda}{\delta - \beta} \beta \delta \sin \beta$$

$$D_{22} = \lambda \alpha (\cosh \beta - \cos \alpha)$$

and

$$\alpha = \sqrt{\Omega + \varepsilon} \quad , \quad \beta = \sqrt{-\Omega + \varepsilon}$$

$$\Omega = \frac{b^2(s^2 + R^2)}{2} \quad , \quad \varepsilon = b\sqrt{\frac{b^2}{4}(s^2 + R^2)^2 - (b^2 s^2 R^2 - 1)}$$

$$b^2 = \frac{\rho A' \omega^2 L^4}{EI}, \quad s^2 = \frac{EI}{k'A'G'L^2}, \quad R^2 = \frac{I}{A'L^2}$$

The natural frequencies of a beam element, ω_r of r-th mode, can be determined using equation (31). Once the natural frequencies are obtained, the r-th mode eigenfunction expression for transverse displacement and rotation, $\tilde{y}_r(x)$ and $\tilde{\varphi}_r(x)$, can be written as

$$\tilde{y}_r \ldots \quad \left\{ C_1 \sin\left(\frac{\alpha_r}{L}x\right) + C_2 \cos\left(\frac{\alpha_r}{L}x\right) + C_3 \sinh\left(\frac{\beta_r}{L}x\right) + C_4 \cosh\left(\frac{\beta_r}{L}x\right) \right\} \tag{32}$$

$$\tilde{\varphi} \ldots \quad \frac{A}{L}\left\{ \lambda_r\left(C_1 \cos\left(\frac{\alpha_r}{L}x\right) - C_2 \sin\left(\frac{\alpha_r}{L}x\right) \right) + \delta_r\left(C_3 \cosh\left(\frac{\beta_r}{L}x\right) + C_4 \sinh\left(\frac{\beta_r}{L}x\right) \right) \right\} \tag{33}$$

where

$$\lambda_r = \alpha_r - \frac{(bs)^2}{\alpha_r} \quad , \quad \delta_r = \beta_r + \frac{(bs)^2}{\beta_r}$$

$$C_1 = L, \quad C_2 = -\frac{D_{11}}{D_{12}}C_1, \quad C_3 = \frac{\alpha_r - \lambda_r}{\delta_r - \beta_r}C_1, \quad C_4 = \frac{\alpha_r \lambda_r}{\delta_r \beta}C_2$$

In the above equations, A_r is the constant which is obtained from the mass normalization of the eigenfunctions in order to satisfy the orthogonality condition:

$$\int_{x=0}^{L} \left\{ \begin{array}{c} \tilde{} \\ \vdots \\ \tilde{} \end{array} \right\}^{T} \left[\begin{array}{cc} \rho A' & 0 \\ 0 & \rho I \end{array} \right] \left\{ \begin{array}{c} \tilde{} \\ \vdots \\ \tilde{} \end{array} \right\} dx = \begin{cases} 1, & s = r \\ 0, & s \neq r \end{cases} \tag{34}$$

Note that since the free-free end conditions have been considered, there are two rigid body modes to be considered:

$$y_0^{trans}(x) = \left. 1 \middle/ \sqrt{\rho A' L} \right., \tag{35}$$

$$\varphi_0^{rot}(x) = \sqrt{\frac{12}{\rho A' L^3}} \left(x - \frac{L}{2} \right) \tag{36}$$

The former expression represents the translational rigid body mode and the latter one represents the rotational rigid body mode. Consider a beam with free end conditions at points 1 and 2 as shown in Figure 3.4. The receptance functions between the linear and rotational displacements (y and φ) and applied forces f and moments M at the end points are defined as:

$$H_{mn} = \frac{y_m}{f_n}, \quad L_{mn} = \frac{y_m}{m_n}, \quad N_{mn} = \frac{\varphi_m}{f_n}, \quad P_{mn} = \frac{\varphi_m}{m_n} \quad ; m,n = 1,2 \tag{37}$$

Figure 3.4. A beam element with free-free end conditions

44

Using the obtained eigenfunction expressions in (32), (33) and the rigid body modes, the receptance functions between the linear and rotational displacements and applied forces f and moments M at the end points, can be determined as the following:

$$H_{mn} = \sum_{r=0}^{\infty} \frac{\tilde{\cdot} \cdots \tilde{\cdot}}{(1+i\gamma)\omega_r^2 - \omega^2} \tag{38}$$

$$L_{mn} = \sum_{r=0}^{\infty} \frac{\tilde{\cdot} \cdots \cdot}{(1+i\gamma)\omega_r^2 - \omega^2} \tag{39}$$

$$N_{mn} = \sum_{r=0}^{\infty} \frac{\tilde{\zeta} \cdots \tilde{\cdot}}{(1+i\gamma)\omega_r^2 - \omega^2} \tag{40}$$

$$P_{mn} = \sum_{r=0}^{\infty} \frac{\tilde{\zeta} \cdots \tilde{\cdot}}{(1+i\gamma)\omega_r^2 - \omega^2} \tag{41}$$

Using the above relations, the direct and cross transfer functions at the ends of beam element can be obtained which are later used for calculating coupled segments' FRF. In the next section, receptance coupling method is presented.

3.3. Receptance coupling

Once the receptance functions of the elements have determined through the equations (38-41), the FRF of coupled segments can be determined through receptance coupling method which is based on compatibility and continuity relations. Consider Figure 3.5 in which two segments A and B are coupled to from a two-segment beam C. To apply the receptance coupling method, first the receptance functions of the elements have to be written in matrix form as

$$[Z] = \begin{bmatrix} [Z_{11}] & [Z_{12}] \\ [Z_{21}] & [Z_{22}] \end{bmatrix}, \quad Z = A, B \tag{42}$$

where the numbers 1 and 2 indicated the end points of each element according to Figure 3.4. The submatrices Z_{ij} include the corresponding receptance functions. For example the first submatrix Z_{11} is defined as

$$[Z_{11}] = \begin{bmatrix} H_{Z11} & L_{Z11} \\ N_{Z11} & P_{Z11} \end{bmatrix} \tag{43}$$
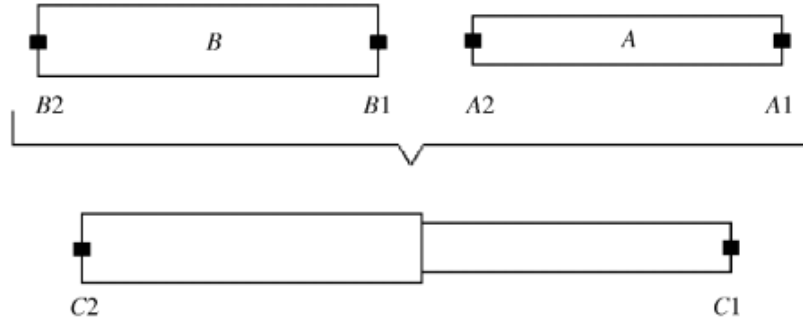
Figure 3.5. Rigid coupling of two beam elements with free-free end conditions [43]

As the receptance matrix for elements A and B are obtained according to equations (42) and (43), the receptance matrices of the resulting beam C are calculated through compatibility and continuity relations as [43]:

$$[C] = \begin{bmatrix} [C_{11}] & [C_{12}] \\ [C_{21}] & [C_{22}] \end{bmatrix} \tag{44}$$

where

$$[C_{11}] = [A_{11}] - [A_{12}][[A_{22}] + [B_{11}]]^{-1}[A_{21}], \tag{45}$$

$$[C_{12}] = [A_{12}] \left[[A_{22}] + [B_{11}] \right]^{-1} [B_{12}],$$ (46)

$$[C_{21}] = [B_{21}] \left[[A_{22}] + [B_{11}] \right]^{-1} [A_{21}],$$ (47)

$$[C_{22}] = [B_{22}] - [B_{21}] \left[[A_{22}] + [B_{11}] \right]^{-1} [B_{12}].$$ (48)

In the above equations, elements are coupled rigidly and contact stiffness and damping are not considered for coupling of elements. However, for elastically coupled components (e.g. for coupling of tool and tool holder), the dynamic parameters should be considered in the interface of two components. This can be done by slightly modifying the equations (45-48) and stiffness matrix. Considering translational stiffness k_y, translational damping c_y, rotational stiffness k_φ and rotational damping c_φ, the complex stiffness matrix is defined as

$$[K] = \begin{bmatrix} k_y + i\omega c_y & 0 \\ 0 & k_\varphi + i\omega c_\varphi \end{bmatrix}$$ (49)

Then, the modified receptance coupling relations can be expressed as

$$[C_{11}] = [A_{11}] - [A_{12}] \left[[A_{22}] + [K]^{-1} + [B_{11}] \right]^{-1} [A_{21}],$$ (50)

$$[C_{12}] = [A_{12}] \left[[A_{22}] + [K]^{-1} + [B_{11}] \right]^{-1} [B_{12}],$$ (51)

$$[C_{21}] = [B_{21}] \left[[A_{22}] + [K]^{-1} + [B_{11}] \right]^{-1} [A_{21}],$$ (52)

$$[C_{22}] = [B_{22}] - [B_{21}] \left[[A_{22}] + [K]^{-1} + [B_{11}] \right]^{-1} [B_{12}].$$ (53)

3.4. Semi-analytical tool point FRF prediction

FRF at the tool tip is a combination of different components' dynamic responses where each component, i.e. spindle, holder and tool, are composed of several segments and substructures. Moreover, the bearing dynamics and joint parameters between these components can also effectively change the dynamic response of system. As previously mentioned, the FRF of a complete spindle-holder-tool assembly including the effect of bearing and joints parameters can be calculated analytically as detailed in [43]. However, this requires accurate modeling and precise information of the each component and its segments. Accessing to the spindle and its internal components, identifying the exact bearing and joints parameters, and simplifying the complex taper structure of holder are tough and time-consuming tasks. In this thesis, the machine tool is considered as two substructures as illustrated in Figure 3.6. The assembly of spindle and holder are considered as one substructure (*SH*) and the tool is the other substructure (*T*). These two substructures are coupled using the tool-holder interface parameters to obtain the dynamic response of the whole structure (*SHT*). To avoid the modelling and contact dynamics identifying errors of spindle-holder assembly, the frequency response of this substructure is obtained experimentally through modal hammer test, while the dynamics of the tool is calculated analytically by modeling it as free-free beam elements.
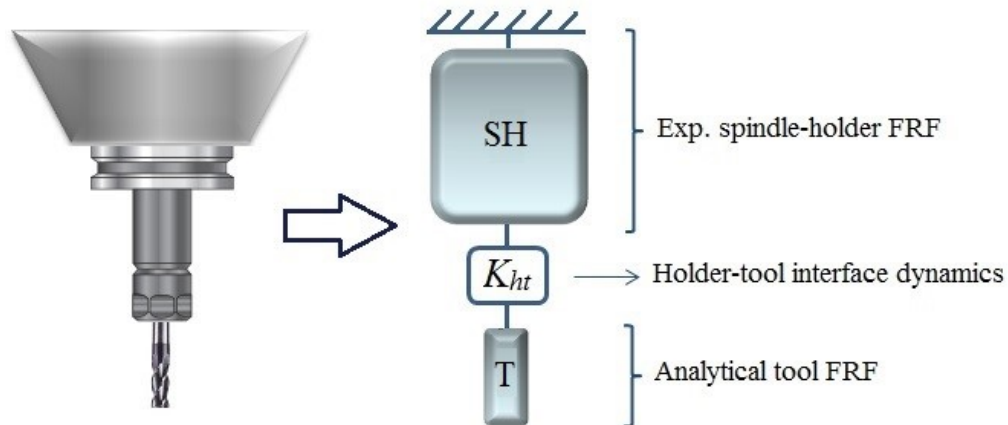
Figure 3.6. Modeling the structure of spindle-holder-tool assembly as two substructures

Once the frequency response of the spindle-holder assembly is measured at the holder tip (SH_{11}) and the direct and crossed FRFs of the tool between the end-coordinates 1 and 2 (T_{11}, T_{12}, T_{21} and T_{22}) are calculated, the FRF of coupled system at the tool tip can be evaluated by the following relation:

$$SHT_{11} = T_{11} - T_{12}(T_{22} + K_{ht}^{-1} + SH_{11})^{-1}T_{21} \tag{54}$$

As it can be seen in Figure 3.6 and in equation (54), the only contact parameters that should be identified are the holder-tool interface parameters which is describe by the matrix K_{ht}. Meanwhile, K_{ht} can be identified through inverse receptance coupling method. For this purpose, the transfer functions at tool tip and holder tip (when the tool is not clamped) should be measured. Then, rearranging equation (54) yields to

$$K_{ht}^{-1} = (T_{12}^{-1}(T_{11} - SHT_{11}^{\text{exp.}})T_{21}^{-1})^{-1} - SH_{11}^{\text{exp.}} - T_{22} \tag{55}$$

Note that in the above equation, SHT_{11} and SH_{11} are experimentally obtained. Once K_{ht} is identified, SHT_{11} can be calculated for any other tool or different overhang lengths.

3.5. Modifying tool tip FRF methodology

In this section, the proposed procedure for damping the flexible tool mode is presented. As mentioned earlier, the objective is to damp the dominant tool mode utilizing the modes of the structure (including the spindle and holder). According to Figure 3.6, the dominant mode of substructure T is damped by the modes of substructure SH. The idea is similar to application of passive vibration absorbers which are attached to a structure to damp the dominant mode. However, here the dominant mode of the structure (the tool mode) is damped by the other modes of the structure itself without using any absorbers or external devices.

The first step of the procedure is to identify the structure's modes which can be done by measuring the FRF at the holder tip, i.e. SH_{11}. Note that the tool should not be clamped to the holder. Examining the experimentally obtained frequency response function, the operative modes that can be used for the damping purpose are identified and the most feasible one is selected which is called f_h hereafter. In the next stage, the tool overhang length is tuned such as the natural frequency of tool mode is close enough to the selected holder-tip mode f_h, so modes interaction occurs and the tool mode damps since its vibrating energy is absorbed by the holder-tip mode. For tuning the tool mode, the FRF of the free-free tool is calculated and elastically coupled to the holder considering the holder-tool interface parameters to obtain the tool-tip FRF. Then the tool-tip FRF is set to be the objective in an optimization algorithm to find the optimum tool length L_{op} leading to a tool mode whose frequency is close to the natural frequency of the holder-tip mode f_h. Using L_{op}, the modified tool-tip FRF with a damped mode is obtained. The objective of the optimization can be obtaining equal magnitude peaks of FRF, similar to Den Hartog's approach, or obtaining equal real troughs similar to Sim's approach in tuning the parameters of tuned mass dampers. Once the optimum length is found, the FRF at the tool tip with the damped tool mode by the holder-tip mode can be obtained.

The proposed method is presented in Figure 3.7. According to this figure, steps of the procedure to damp the tool mode can be summarized as follows:

- Applying hammer impact test to at the tool tip at an arbitrary overhang length to measure $SHT_{11}^{exp.}$,
- Disassembling the tool from the holder and applying hammer impact test to at the tool tip to measure $SH_{11}^{exp.}$,
- identifying K_{ht} from equation (55),
- Determining the operative holder-tip mode,
- Obtaining the optimal tool overhang length L_{op} tuned to the determined holder mode,
- Calculating free-free tool's FRFs (T_{11}, T_{12}, T_{21} and T_{22}) with the obtained overhang length,

- Coupling substructures *T* and *SH* elastically using the identified holder-tool interface parameters through equation (54) to obtain the optimal FRF at the tool-tip SHT_{11}.

```
┌──────────────────────────────┐   ┌──────────────────────────────┐
│ Spindle-holder-tool Assembly │   │  Spindle-holder assembly     │
│ with an arbitrary tool       │   │  (the tool is not clamped)   │
│ overhang length              │   │                              │
└──────────────────────────────┘   └──────────────────────────────┘

        ┌──────────────────────────────────────────────┐
        │ FRF Measurement through hammer impact test    │
        └──────────────────────────────────────────────┘

   ┌──────────────────────────┐        ┌──────────────────────────────┐
   │ Inverse receptance       │        │ Determining the target mode  │
   │ coupling                 │        │ at the holder-tip and the    │
   └──────────────────────────┘        │ operative frequency range    │
                                       └──────────────────────────────┘
          ┌──────┐                     ┌──────────────────────────────┐
          │ K_ht │                     │ Analytical FRF of free-free  │
          └──────┘                     │ tool in the determined range │
                                       │ (with corresponding lengths) │
                                       └──────────────────────────────┘

              ┌──────────────────────────────┐
              │   Receptance coupling         │
              └──────────────────────────────┘

                 ┌──────────────────────────┐
                 │ Tuned overhang           │
                 │ length L_op.             │
                 └──────────────────────────┘

                 ┌──────────────────────────┐
                 │ Modified tool-tip FRF     │
                 │ with damped tool mode     │
                 └──────────────────────────┘
```
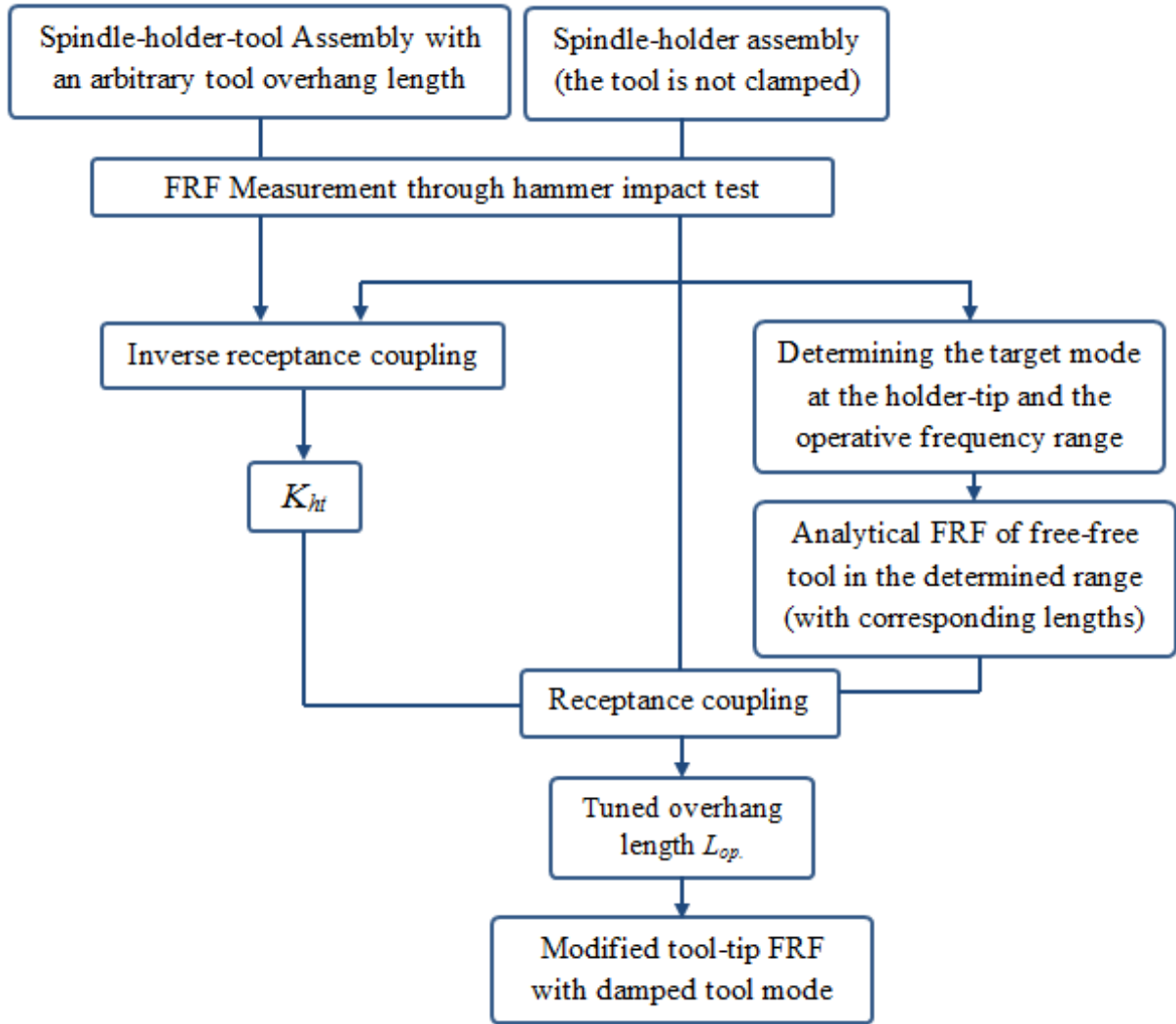
Figure 3.7. Developed procedure of tool-tip FRF modifying

3.6. Simulations and experimental results

In this section, the tuning methodology discussed in the previous section is used to damp a dominant mode of a milling machine tool system. The transfer function of the tool with an arbitrary overhang length (56 mm) is shown in Figure 3.8-a which has been obtained

experimentally through hammer test. The tool is a 12 mm diameter carbide endmill. A dominant mode with high flexibility is visible around 3000 Hz. A simple modal shape analysis has been done using measured FRFs at the tool tip and the holder tip. The resulting mode shapes shown in Figure 3.8-b reveals that the dominant mode belongs to the tool since the tool deflects too much at this mode while the displacement of the tool at the first mode is mainly due to the deflection of the holder and they are along the same direction.
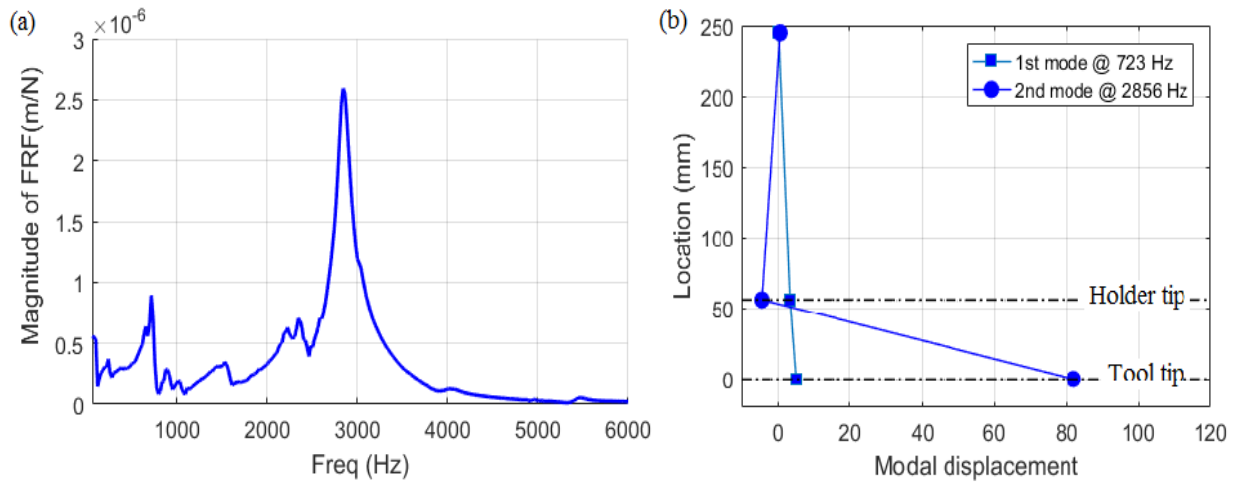
Figure 3.8. a) Measured tool-tip FRF b) mode shapes

Then, the tool has been disassembled and FRF of the structure at the holder tip (without the tool) is measured as given in Figure 3.9. As it can be seen, there are several operative modes that can be used to damp the tool mode. However, the focus is on modes which are close enough to the tool mode in Figure 3.8. The closest holder-tip modes to tool mode (which was around 3000 Hz) are around 2500 Hz and 4000 Hz, at the left and right hand side of the tool mode, respectively. For our case, the latter one, i.e. the mode at 4000 Hz, is selected.

Figure 3.9. Holder-tip FRF (the tool is not clamped)

Once the target mode at the holder-tip is selected, the next step is to tune the tool length so that the tool mode is tuned to the holder-tip mode leading to modes interaction and damping of the tool mode. Regarding the numerical optimization, a frequency range $[f_0\ f_1]$ arou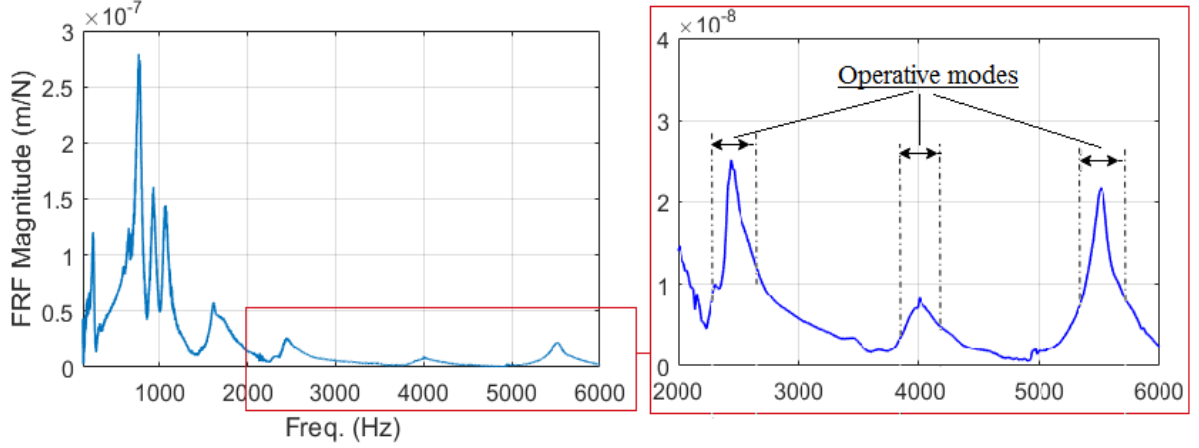nd f_h is set to be the range of searching for the optimized tool overhang length L_{op}. For our case, f_0 and f_1 were set to be 3600 Hz and 4400 Hz, respectively. The corresponding lengths, L_0 and L_1, to the frequencies f_0 and f_1 can be obtained from equation (31) numerically or can be estimated by Euler Bernouli beam relation since it provides an explicit formula between the natural frequency and length of the beam:

$$\omega = \sqrt{\frac{EI}{\rho A}} \left(\frac{(2n+1)\pi}{2L} \right)^2 \tag{56}$$

The optimized length L_{op} was obtained numerically in the software MATLAB using the function **fminsearch** as 43 mm, based on equal peaks approach. To avoid significant numerical errors, a tolerance of 1e-12 was selected. Using the calculated L_{op}, the modified FRF can be obtained by analytically calculating the tool transfer functions and coupling it to the experimental transfer function at the holder tip using the contact parameters. Figure 3.10 shows the resulting FRFs where the optimization objective is obtaining equal peaks. The red line shows the free-free tool's FRF when it is elastically coupled to a wall using

53

K_{ht}. As it can be seen, there is a dominant mode around 4000 Hz with a remarkable flexibility. However, when it is clamped to the holder-tip FRF the dominant mode splits into two smaller modes at the two sides. This is due to the interaction between the tool mode (red) and the target mode at the holder-tip (the operative mode in Figure 3.9) which yields to a damping effect and suppression of the tool mode, resulting in a modified tool-tip FRF (the blue line).
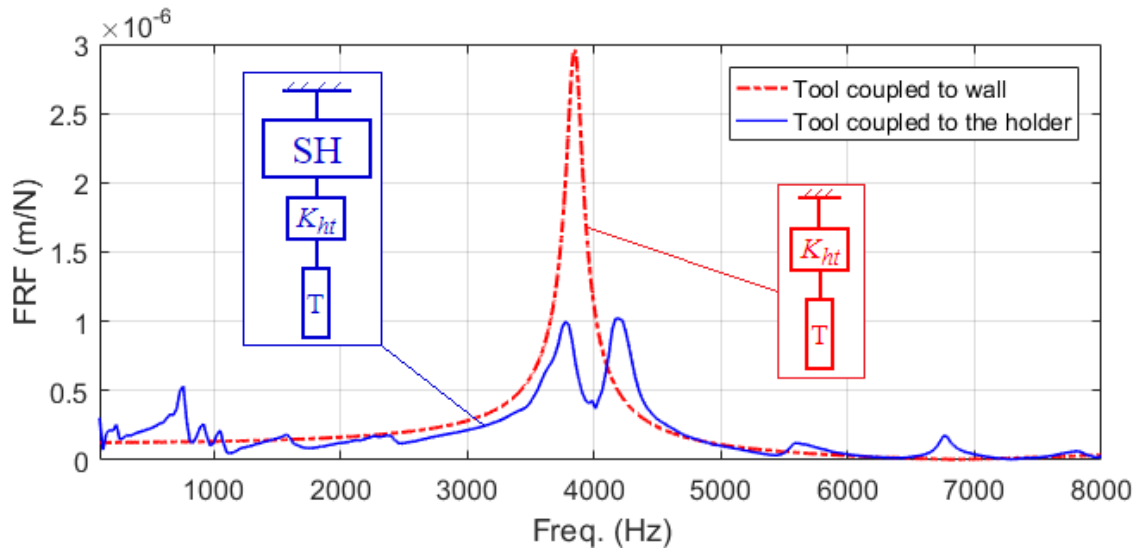
Figure 3.10. Simulated tool-tip FRF with the optimized tool length

The modified tool-tip FRF using the obtained L_{op} is experimentally verified in Figure 3.11. Compared to the previously measured FRF with an arbitrary overhang length, more than two times reduction in the maximum magnitude of the transfer function has been obtained which is very effective in enlarging the stable zone. The corresponding stability lobes using experimental FRFs are also given in Figure 3.12 which shows noticeable improvement in stability limit of the system. The cutting tests are conducted for half immersion of AL7075 with the Carbide endmill with diameter of 12 mm and arbitrary and optimized overhang lengths, i.e. 56 mm and 43 mm respectively. The sound spectrum and photo of surface after cutting are given in Figure 3.13 at axial depths of 1.3 mm and 2.3 mm. It can be seen that at cutting depth of 1.3 mm, cutting with arbitrary length is unstable and chatter marks are

54

visible at the cut surface (Figure 3.13-c). However, cutting at the same axial depth with the optimized tool overhang length is stable and chatter has not developed (Figure 3.13-b).
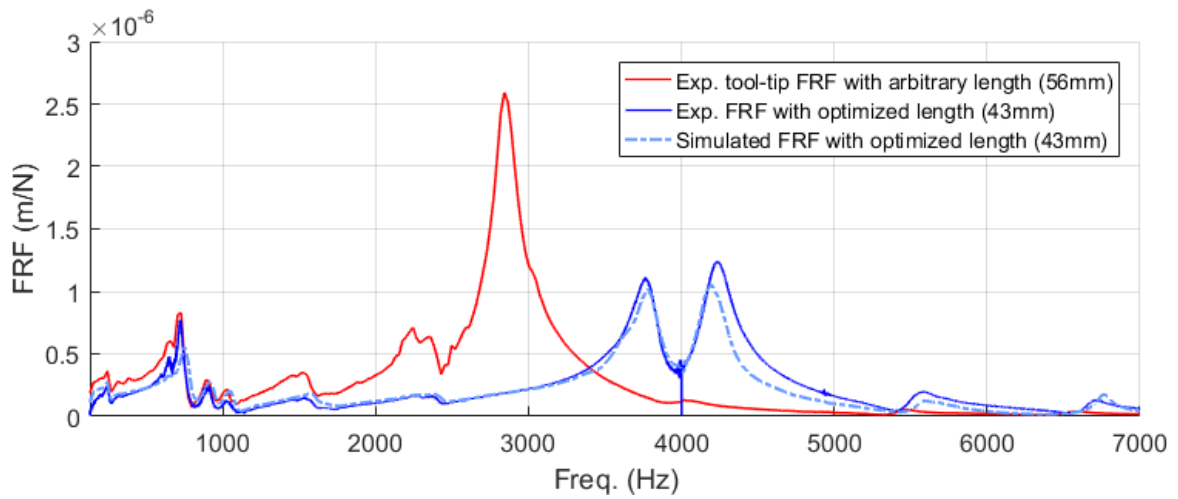
Figure 3.11. Experimental tool-tip FRF with the optimized tool length
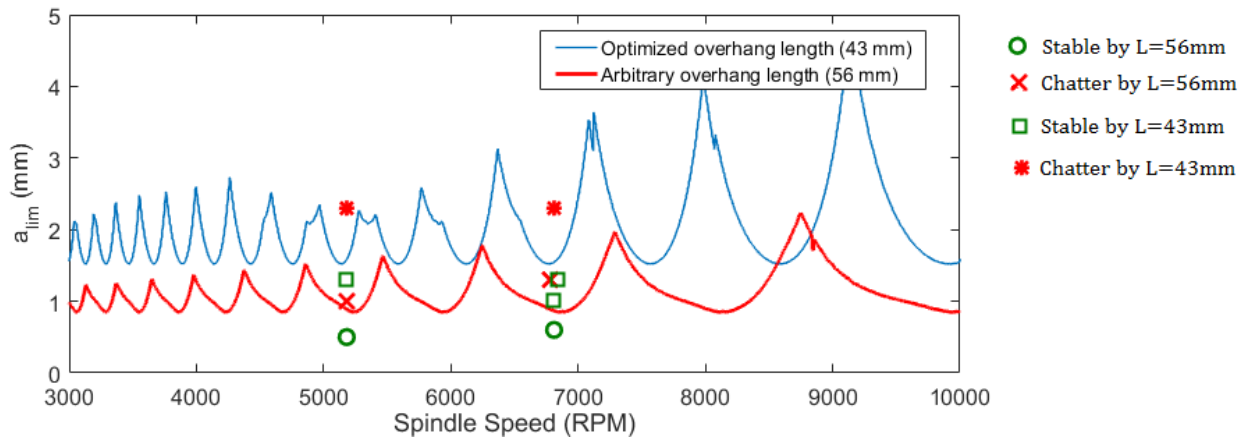
Figure 3.12. Stability lobe diagrams for the arbitrary tool overhang length of 56 mm and optimized length of 43 mm.
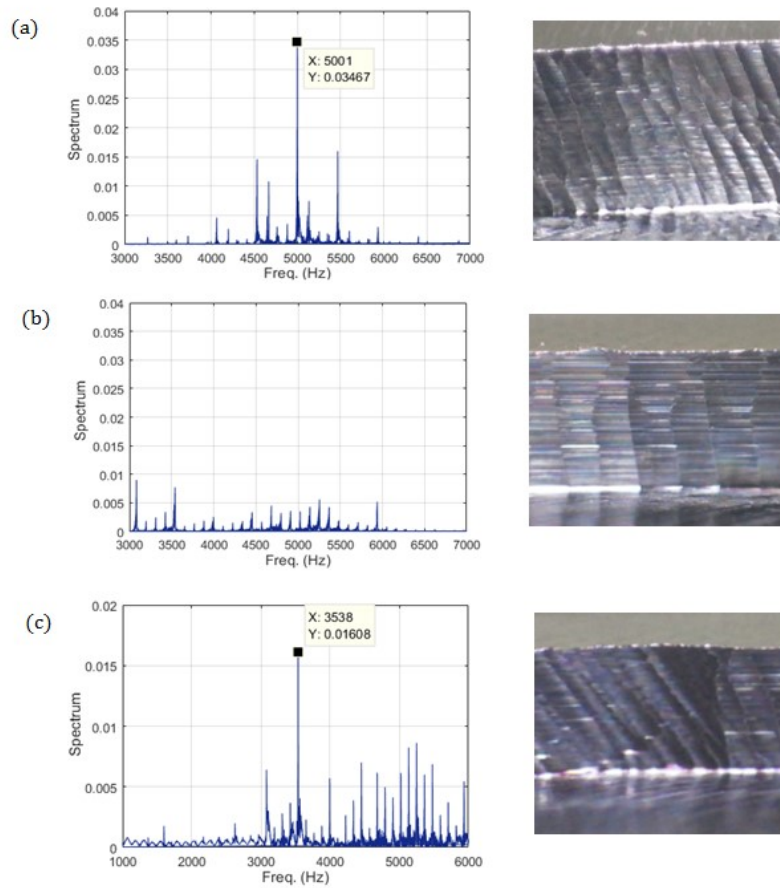
Figure 3.13. Sound spectrum and surface photo at 6811 rpm and a) 2.3 mm axial depth with 43 mm overhang length, b) 1.3 mm axial depth with 43 mm overhang length, c) 1.3 mm axial depth with 56 mm overhang length.

For calculating the L_{op} and the resulting modified FRF in Figure 3.10, the objective was to minimize the transfer function magnitude and to obtain equal peaks. However, the objective function can be maximizing the most negative real part of transfer function which leads to equal real troughs. Thus, the simulations for the equal troughs objective have been done and the results are presented in Figure 3.14. The calculated L_{op} based on this approach was 45.6 mm.

56

Figure 3.14. Tool-tip FRFs based on equal peaks and equal real troughs approaches.

3.7. Conclusion

Improving material removal rate is among top priorities of manufacturing industries which can be reached by enlarging stable cutting zone during machining. For this purpose, many researches have focused on modifying the dynamics of structures through different approaches. As mentioned in the first chapter, the main objective of the second part of this thesis was to take advantage of multi-mode dynamics of systems in order to enlarge the stable cutting zone.

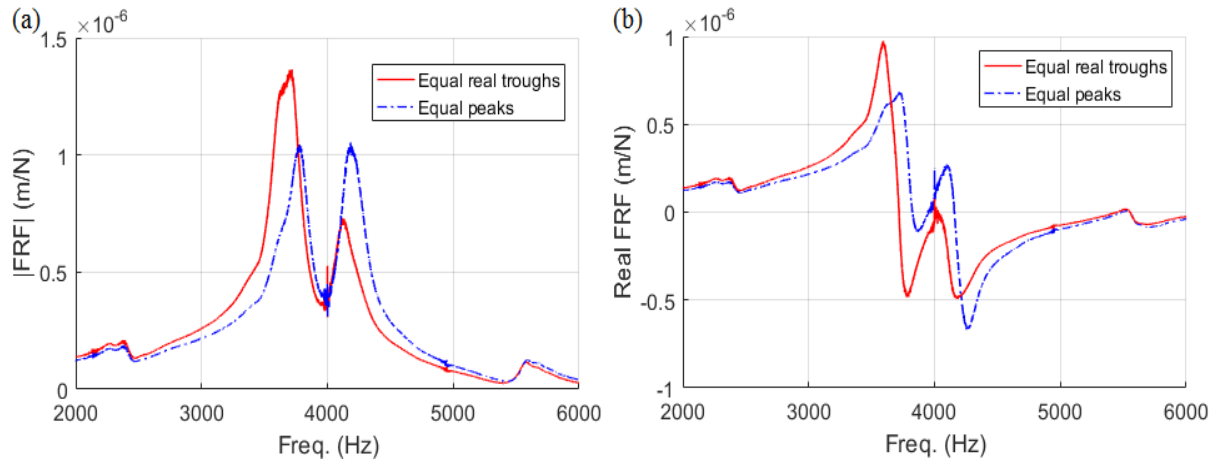In this section, a new approach to passively modify the dynamic response of the system, i.e. the frequency response function, without using any external devices but by utilizing the structure modes was discussed. A procedure was presented to tune the tool mode such a way that it is damped by the modes of the structure emerged at the holder-tip. The developed method was based on coupling of tool's FRF and FRF at the holder tip through receptance coupling method. The tool's FRFs were calculated analytically through beam analysis while the FRF of the holder tip was experimentally measured through hammer test. It was shown that the flexibility of the tool's dominant mode can significantly decrease if the tool is clamped with the optimum overhang length. Once the tool is clamped with the optimum overhang length, the tool mode shifts towards the target mode at the holder-tip and modes interaction occurs. As a result, vibrating energy of the tool mode is absorbed by

57

the holder-tip mode; the tool mode is suppressed and its magnitude decreases. Note that the tool mode can shifts towards the target mode by changing the other tool dimensions such as tool diameter instead of overhang length. However, since changing the overhang length is more practical, it has been selected as variable parameter.

The simulation results were verified through hammer tests and good agreement were observed between predicted and experimental results. For the experimental study case, a reduction of more than 200% was observed in the magnitude of tool-tip FRF. Through this procedure, only a single impact test at the holder tip is required (to avoid complex modeling of holder and spindle's segments) which makes the FRF predicting procedure for different tools and lengths more efficient. The effect of tool-tip FRF modifying on stability of the system was illustrated by constructing the corresponding stability lobes diagrams which showed remarkable improvement is the stable cutting depths, and consequently in material removal rate.

Although the simulations and experiments were done on a milling system, the presented idea and procedure can be applied to other systems and implemented on different machine tools as well, such as a turning machine. In a structure with multiple components, once the vibration modes of a component are identified, the modes of the other components can be modified by tuning them properly.

Chapter 4 **SUMMARY OF THESIS**

Dynamics of machining systems are the primary and most crucial information which determine their stability/instability behavior for specific cutting conditions. In this thesis, the focus was on investigating the effects of multiple modes of systems and their significance. In this regard, two topics have been studied about effects of multi-mode dynamics of system on stability. First, the stability behavior of milling systems at low cutting speeds where process damping is dominant has been investigated. In the second part of the research, FRF modification of a system through its multi-mode dynamic characteristics has been studied.

The first part of thesis is concerning the process damping effect in multi-mode milling systems. The stability of milling systems with well separated modes at relatively low and high frequencies has been explored. Stability lobes diagrams have been constructed for each mode separately though analytical frequency domain solution. Then, the lowest envelopes of the diagrams are selected as the ultimate stability frontier. Moreover, simulations have been done for vibration of the cutting tool in time domain considering multiple modes simultaneously. In the time domain model, process damping effect is introduced as a ploughing cutting force as a function of indentation volume.

It has been shown that the amount of generated process damping of different modes is different due to their frequencies. Low frequency modes produce less process damping while high frequency modes offer more process damping. This is due to the different wavy surfaces that they generate. Low frequency mode generates a smoother wavy surface with less slope which leads to fewer indentation and less process damping. As a result, stability limits corresponding to low frequency modes cannot increase as high frequency modes and they can cause chatter at cutting depths which were expected to be stable with the assumption of single mode system.

Simulation and experimental results showed that even if low frequency modes are much more rigid and offer high stability limits at high cutting speeds, chatter can develop at these modes instead of more flexible modes at higher frequencies. Indeed, the high frequency

modes can suppress themselves due to high process damping and as a result, the corresponding stability limits shift up much more than stability limits of low frequency modes. Thus, the stability limits of these modes can cross out each other and chatter mode shifts from high frequency mode to low frequency mode as cutting speed decreases. The time domain simulation results showed despite the fact that flexible high frequency mode dominate the cutting tool vibration at stable cutting zone, chatter can develop at the rigid low frequency modes.

From the resulting stability limits, it can be concluded that rigid modes at low frequencies must not be ignored while predicting the stability frontier. Focus of researchers and machine tool users should be on damping of such modes for increasing material removal rate even if their rigidities are much more compared to other modes at higher frequencies. Considering this, if someone wants to use an absorber for example, it should be tuned to the low frequency modes, not the most flexible ones at higher frequencies. Another way to increase the material removal rate is to increase the process damping effect by changing the tool geometry. This can be done by increasing nose radius of the cutter, decreasing the clearance angle, or by using a tool with cylindrical flank face rather than planar flank face. Other than these, the low frequency modes can be moved to higher frequencies by modifying the structure, which results in higher process damping effect.

In the second part of this thesis, the focus is on modifying dynamic response of structures, i.e. frequency response function, in order to increase the stability limit and enlarge the stable cutting zone. A procedure was developed to properly suppress a dominant tool mode on a milling machine tool by changing the tool dimensions, i.e. the overhang length. Using this procedure, the optimized tool overhang length can be found considering the identified structure's modes at the holder tip through hammer impact test. FRF of the tool with free-free boundary conditions has been calculated using beam element theory and it has been elastically coupled to the experimentally obtained FRF at the holder tip through receptance coupling method.

Using the optimized tool overhang length, the tool mode takes place close to a mode of structure at the holder tip which leads to modes interaction. Due to the modes interaction, the vibration energy of dominant tool mode is absorbed by the holder-tip mode and it is

suppressed. An experimental case on a milling machine tool has been conducted and it is observed that the tool-tip FRF of system can be reduced to less than half. This remarkable reduction in FRF can shifts the stability frontier up and enlarges the stable cutting zone as illustrated for the experimental case.

Original contributions

Process damping has been previously studied in several researches for single mode systems where the effects of other modes were ignored. However, this research emphasized the effect of vibration frequency on process damping by taking into account all modes of the system. The frequency domain solution for milling stability with process damping effect given in [29] is generalized to systems with multiple modes. Apart from frequency domain solution, a time domain milling model was developed with respect to dynamics of multiple modes simultaneously which includes the effect of process damping compared to other models for multi-mode milling systems.

The presented tool-tip FRF suppression method was based on a new approach compared to other methods in the literature. To the author's knowledge, re-designing structures (topology optimizations) and using passive or active vibration absorbers are the common methods to modify FRF of systems. However, the methodology developed in this thesis utilizes the multi-mode characteristics of systems and FRF modification is done by using the modes of the structure itself without any requirement for changing the structure design or using any external devices, such as TMDs. This method is based on tuning and interaction of the already existing structure modes.

Recommendations for future research

Within the scope of this study, in the frequency domain solution, the stability lobes are calculated separately for each dominant mode with the process damping effect. However, considering the nonlinear effect of process damping, further improvements of the frequency domain model by considering the effects of multiple modes simultaneously may increase the fidelity of the current model.

Although the dominant mode of a cutting tool on a milling machine tool was suppressed in this study, the presented procedure for FRF modification can be easily implemented on other systems and machine tools. For example in boring and turning machining, where there is normally a flexible mode of cutting tool, the structure modes can act as a dynamic vibration absorber. Moreover, application of the presented approach in robotic machining can be greatly rewarding as the dimensions of different components of robotic machines and their corresponding dynamic modes can be easily tuned and it is more feasible to benefit from their interaction compared to CNC machine tools.

BIBLIOGRAPHY

[1]   Quintana G, Ciurana J. Chatter in machining processes: a review. International Journal of Machine Tools and Manufacture. 2011 May 31;51(5):363-76.

[2]   J. Tlusty and M. Polacek, "The stability of machine tools against self-excited vibrations in machining," Int. Res. Prod. Eng., vol. 1, no. 1, pp. 465–474, 1963.

[3]   H. E. Merritt, "Theory of self-excited machine tool chatter," J. Eng. Ind., vol. 87, no. 4, pp. 447–454, 1965.

[4]   Tobias SA. Machine tool vibration. Blackie and Sons Ltd, New York; 1965.

[5]   F. Koenigsberger and J. Tlusty, Machine tool structures. Elsevier, 2016.

[6]   Minis I. and Yanushevsky T. A New Theoretical Approach for the Prediction of Machine Tool Chatter in Milling, ASME Journal of Engineering for Industry; 1993. 115, 1-8.

[7]   Altintas Y, Budak E. Analytical prediction of stability lobes in milling. Trans ASME J Eng Ind; 1995. 44:357–362.

[8]   Budak E, Altintas Y. Analytical prediction of chatter stability in milling—part I: general formulation. Journal of dynamic systems, measurement, and control. 1998 Mar 1;120(1):22-30.

[9]   Mann BP, Young KA, Schmitz TL, Dilley DN. Simultaneous stability and surface location error predictions in milling. Journal of Manufacturing Science and Engineering. 2005 Aug 1;127(3):446-53.

[10]   Berglind, Luke, and John Ziegert. "Analytical time-domain turning model with multiple modes." CIRP Annals-Manufacturing Technology 64.1 (2015): 137-140.

[11]   Tang WX, Song QH, Yu SQ, Sun SS, Li BB, Du B, Ai X. Prediction of chatter stability in high-speed finishing end milling considering multi-mode dynamics. J Mater Process Technol; 2009. 209: 2585–2591.

[12] Wan M, Ma YC, Zhang WH, Yang Y. Study on the construction mechanism of stability lobes in milling process with multiple modes. Int J Adv Manuf Technol; 2015. 79:589–603.

[13] Takemura T, Kitamura T, Hoshi T. Active Suppression of Chatter by Programed Variation of Spindle Speed. Journal of the Japan Society of Precision Engineering. 1975 May 5;41(484):489-94.

[14] Budak E. An analytical design method for milling cutters with non-constant pitch to increase stability, part I: theory. Transactions-American Society of Mechanical Engineering Journal of Manufacturing Science and Engineering. 2003 Feb 1;125(1):29-34.

[15] Yusoff AR, Sims ND. Optimisation of variable helix end millings tools by minimising self-excited vibration. In Journal of Physics: Conference Series 2009 (Vol. 181, No. 1, p. 012026). IOP Publishing.

[16] Sisson, T.R. and R.L. Kegg, An explanation of low-speed chatter effects. Journal of Engineering for Industry, 1969. 91(4): p. 951-958.

[17] Das, M.K, Tobias S.A., The Relation Between the Static and the Dynamic Cutting of Metals, International Journal of Machine Tool Design and Research, 763, 89, 1967.

[18] Tlusty J, Ismail F. Special aspects of chatter in milling. Journal of Vibration, Acoustics, Stress and Reliability in Design. 1983 Jan 1;105(1):24-32.

[19] Wu DW. A new approach of formulating the transfer function of dynamic cutting processes. J. Eng. Ind. (Trans. ASME). 1989 Feb 1;111(1):37-47.

[20] Elbestawi, M.A., Ismail, F., Du, R., Ullagaddi, B.C., Modeling Machining Dynamics Including Damping in the Tool-Workpiece Interface, Journal of Engineering for Industry, 116, 435-439, 1994.

[21] Chiou RY, Liang SY. Chatter stability of a slender cutting tool in turning with tool wear effect. International Journal of Machine Tools and Manufacture. 1998 Mar 31;38(4):315-27.

[22] Altintas Y, Montgomery D. Mechanism of cutting force and surface generation in dynamic milling. Journal of Engineering for Industry. 1991 May;113(2):160-8.

[23] Clancy BE, Shin YC. A comprehensive chatter prediction model for face turning operation including tool wear effect. International Journal of Machine Tools and Manufacture. 2002 Jul 31;42(9):1035-44.

[24] Eynian M, Altintas Y. Chatter stability of general turning operations with process damping. Journal of Manufacturing Science and Engineering. 2009 Aug 1;131(4):041005.

[25] Ahmadi K, Ismail F. Analytical stability lobes including nonlinear process damping effect on machining chatter. International Journal of Machine Tools and Manufacture. 2011 Apr 30;51(4):296-308.

[26] Ranganath S, Liu D, Sutherland JW. A comprehensive model for the flank face interference mechanism in peripheral milling. Transactions-north American Manufacturing Research Institution of SME. 1998:249-54.

[27] Huang CY, Wang JJ. Mechanistic modeling of process damping in peripheral milling. Journal of Manufacturing Science and Engineering. 2007 Feb 1;129(1):12-20.

[28] Altintas, Y., Eynian, M., Onozuka, H. Identification of dynamic cutting force coefficients and chatter stability with process damping. CIRP Annals – Manufacturing Technology; 2008. 57/1, 371-374.

[29] Budak E, Tunc LT. Identification and modeling of process damping in turning and milling using a new approach. CIRP Annals-Manufacturing Technology. 2010 Dec 31;59(1):403-8.

[30] Tunç LT, Budak E. Effect of cutting conditions and tool geometry on process damping in machining. International Journal of Machine Tools and Manufacture. 2012 Jun 30;57:10-9.

[31] Chandiramani NK, Pothala T. Dynamics of 2-dof regenerative chatter during turning. Journal of sound and vibration. 2006 Feb 21;290(1):448-64.

[32] Jin X, Altintas Y. Chatter stability model of micro-milling with process damping. Journal of manufacturing science and engineering. 2013 Jun 1;135(3):031011.

[33] Ahmadi K, Altintas Y. Identification of machining process damping using output-only modal analysis. Journal of Manufacturing Science and Engineering. 2014;136(5):051017.

[34] Seguy S, Dessein G, Arnaud L. Surface roughness variation of thin wall milling, related to modal interactions. International Journal of Machine Tools and Manufacture. 2008 Mar 31;48(3):261-74.

[35] Munoa J, Dombovari Z, Mancisidor I, Yang Y, Zatarain M. Interaction between multiple modes in milling processes. Machining Science and Technology, 2013. 17(2):165-80.

[36] Tunç LT, Budak E. Identification and modeling of process damping in milling. Journal of Manufacturing Science and Engineering. 2013 Apr 1;135(2):021001.

[37] Pedersen NL. Maximization of eigenvalues using topology optimization. Structural and multidisciplinary optimization. 2000 Aug 1;20(1):2-11.

[38] Law M, Altintas Y, Phani AS. Rapid evaluation and optimization of machine tools with position-dependent stability. International Journal of Machine Tools and Manufacture. 2013 May 31;68:81-90.

[39] Altintas Y, Brecher C, Weck M, Witt S. Virtual machine tool. CIRP Annals-manufacturing technology. 2005 Jan 1;54(2):115-38.

[40] Mahnama M, Movahhedy MR. Prediction of machining chatter based on FEM simulation of chip formation under dynamic conditions. International journal of machine tools and manufacture. 2010 Jul 31;50(7):611-20.

[41] Garitaonandia I, Fernandes MH, Albizuri J. Dynamic model of a centerless grinding machine based on an updated FE model. International Journal of Machine Tools and Manufacture. 2008 Jun 30;48(7):832-40.

[42] Song QH, Wan Y, Yu SQ, Ai X, Pang JY. Stability prediction during thin-walled workpiece high-speed milling. InAdvanced Materials Research 2009 (Vol. 69, pp. 428-432). Trans Tech Publications.

[43] Ertürk A, Özgüven HN, Budak E. Analytical modeling of spindle–tool dynamics on machine tools using Timoshenko beam model and receptance coupling for the prediction of tool point FRF. International Journal of Machine Tools and Manufacture. 2006 Dec 31;46(15):1901-12.

[44] Da Silva MM, Venter GS, Varoto PS, Coelho RT. Experimental results on chatter reduction in turning through embedded piezoelectric material and passive shunt circuits. Mechatronics. 2015 Aug 31;29:78-85.

[45] Matsubara A, Maeda M, Yamaji I. Vibration suppression of boring bar by piezoelectric actuators and LR circuit. CIRP Annals-Manufacturing Technology. 2014 Dec 31;63(1):373-6.

[46] Dohner JL, Lauffer JP, Hinnerichs TD, Shankar N, Regelbrugge M, Kwan CM, Xu R, Winterbauer B, Bridger K. Mitigation of chatter instabilities in milling by active structural control. Journal of sound and vibration. 2004 Jan 6;269(1):197-211.

[47] Browning DR, Golioto I, Thompson NB. Active chatter control system for long-overhang boring bars. In Proceedings of Smart Structures and Materials Conference 1997 May 23 (pp. 3044-26).

[48] Miguelez MH, Rubio L, Loya JA, Fernández-Sáez J. Improvement of chatter stability in boring operations with passive vibration absorbers. International Journal of Mechanical Sciences. 2010 Oct 31;52(10):1376-84.

[49] Saffury J. Chatter Suppression of External Grooving Tools. Procedia CIRP. 2017 Dec 31;58:216-21.

[50] Tarng YS, Kao JY, Lee EC. Chatter suppression in turning operations with a tuned vibration absorber. Journal of materials processing technology. 2000 Sep 7;105(1):55-60.

[51] Yang Y, Munoa J, Altintas Y. Optimization of multiple tuned mass dampers to suppress machine tool chatter. International Journal of Machine Tools and Manufacture. 2010 Sep 30;50(9):834-42.

[52] Wang M. Feasibility study of nonlinear tuned mass damper for machining chatter suppression. Journal of Sound and Vibration. 2011 Apr 25;330(9):1917-30.

[53] Madoliat R, Hayati S, Ghalebahman AG. Investigation of chatter suppression in slender endmill via a frictional damper. Scientia Iranica. 2011 Oct 31;18(5):1069-77.

[54] Hartog DJ. Mechanical vibrations. McGraw-Hill Book Company; 1956.

[55] Sims ND. Vibration absorbers for chatter suppression: a new analytical tuning methodology. Journal of Sound and Vibration. 2007 Apr 3;301(3):592-607.

[56] Aristizabal-Ochoa JD. Timoshenko beam-column with generalized end conditions and non-classical modes of vibration of shear beams. Journal of Engineering Mechanics. 2004 Oct;130(10):1151-9.